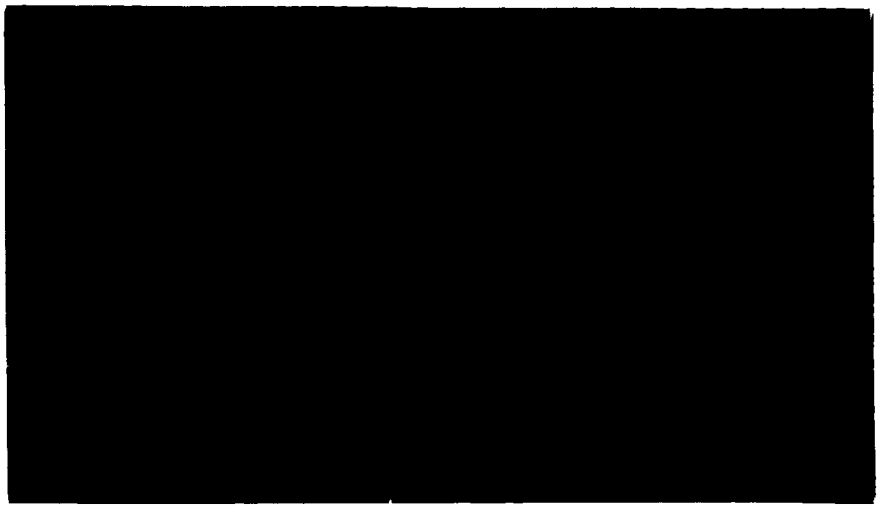

RADIO ASTRONOMY OBSERVATORY

DEPARTMENT OF PHYSICS

FLORIDA STATE UNIVERSITY

TALLAHASSEE, FLORIDA

A STUDY OF POLARIZATION OF DECAMETER RADIATION FROM JUPITER

by

DENIS P. MORROW

A Thesis
Submitted to the Graduate School of
Florida State University in partial
fulfillment of the requirements for
the degree of Master of Science

This thesis is dedicated to
my father

ACKNOWLEDGMENTS

I wish to thank Professor Colin H. Barrow for suggesting this problem and for his aid and advice during the course of the work, Mr. George M. Resch for a suggestion about the error analysis, Mr. James D. Merritt for his assistance with the computer programming, and all those who helped with the reduction of data.

Thanks are also extended to Mrs. Mary D. West for typing the manuscript, to the National Aeronautics and Space Administration (Grant Number NSG-224-61) for supporting this research, and to my wife, Carolyn, for her patience.

TABLE OF CONTENTS

LIST OF TABLES

LIST OF FIGURES

Figures Page

I. INTRODUCTION

The planets of the solar system, until 1954, had been considered comparatively uninteresting objects, visible only by reflected sunlight or thermal emission due to solar heating. The thermal emission is greatest in the infrared region and follows the Rayleigh-Jeans radiation law in the microwave region. It was to be expected that large antennas and sensitive receivers operating at microwave frequencies could detect this thermal emission, and this eventually proved to be the case.[1,2,3]

Prior to this, however, the accidental discovery in 1954 by Burke and Franklin[4] of intense bursts of radiation from Jupiter at 22 Mc/s stimulated the whole science of planetary radio astronomy. The detection of radiation in the decameter region rather than the microwave region was totally unexpected and indicated that at least one planet had an energy source whose interaction with the sun, if any, was not immediately obvious.

This discovery was soon confirmed by Shain,[5] who also introduced an important method of analysis of the Jupiter radiation. Shain's work is shown in Fig. 1 applied to Jupiter noise storms found on records of galactic noise made in 1951. Fig. 1a shows a recurrence tendency

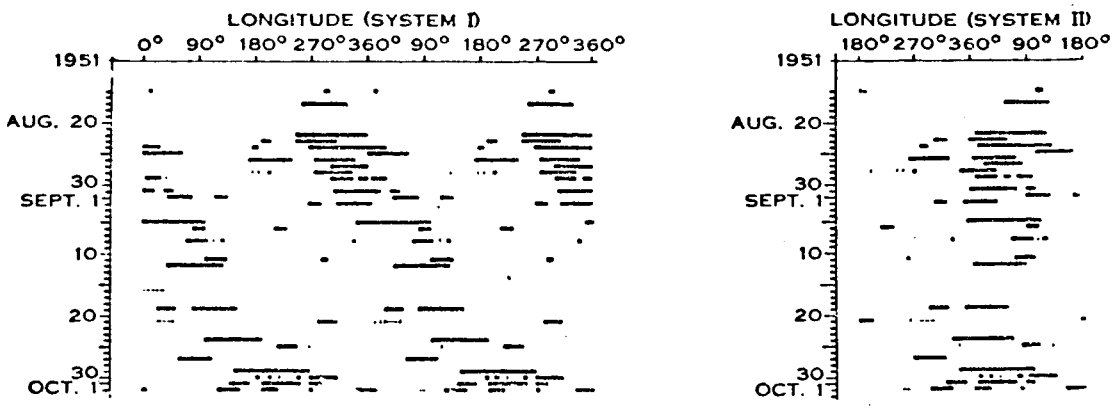

Fig. 1a--Jupiter events in 1951 according to Shain.

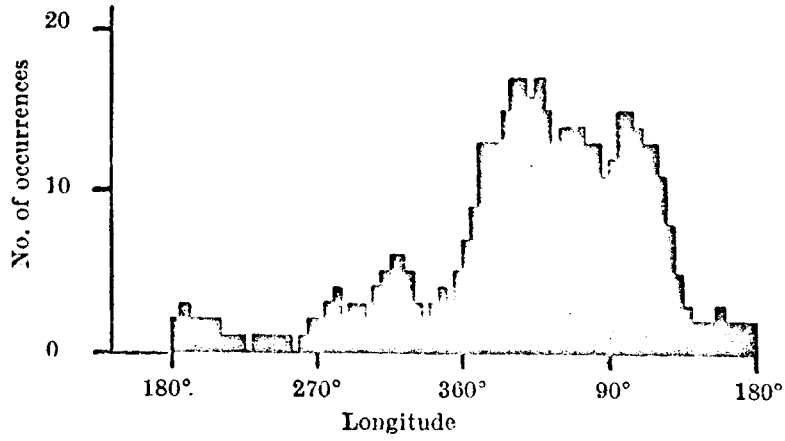

Fig. 1b--Number of occurrences versus System II Longitude for Shain's 1951 data.

for the radiation in System II longitude.* The gradual shift to lower longitudes indicates that the period of the recurrence tendency is very slightly less than the System II rotation period. The histogram in Fig. 1b is a superposition of the activity periods in Fig. 1a. Such histograms of later observations using System II longitude permit precise statistical determinations[6,7] of the drift rate, and hence the rotation period, of the radio sources. This radio rotation rate forms the basis of the System III (1957.0) longitudes now in common use.†

Continued observations have disclosed that the decameter radiation is quite complex. Only two of the proposed theories have gained notable support. A successful theory must explain the following characteristics of the decameter radiation:

1. The intensity of the radiation is greater than that of any cosmic radio source and often rivals that of the disturbed sun.

---

*Visual features in the Jovian atmosphere exhibit differential rotation with well-defined periods. Ephemerides for physical observations of Jupiter use two average central meridian longitude systems, denoted by System I and System II, corresponding to rotation periods of $9^h50^m30.^s004$ and $9^h55^m40.^s632$ respectively.

†The International Astronomical Union in 1962 defined System III central meridian longitudes (λ_{III}) as:[8]

Epoch 1957.0 Julian Date 2435839.5

Radio System III $\lambda_{III(1957.0)}$ $9^h55^m29.^s37$

2. The radiation is sporadic and, when it occurs, consists of a series of bursts known as an event,* which may last for several minutes to several hours. Individual bursts range from about half a second to some ten seconds or longer in duration. Very short signals known as I-pulses,[9] or 'spitting pulses',[10] have durations of fifty milliseconds or less.

3. Noise storms have been observed at frequencies between 4.8 and 38.5 Mc/s,[11,12] although they occur most often below 20 Mc/s.

4. Above 20 Mc/s the radiation is almost exclusively polarized in the right-handed sense. Below 20 Mc/s the proportion of left-handed polarization becomes significantly larger.

5. The more important features of the occurrence probability histograms persist from year to year.† Recent observations indicate that the radio rotation period is lengthening slightly.[14]

Early Jupiter observations concentrated on gathering a large amount of data to obtain a statistically good value for the radio rotation period and on studying the histograms of frequency of occurence versus

---

*At a conference of Jupiter observers at NASA Goddard Space Flight Center in April, 1965, the following definitions were tentatively agreed upon:[13]

1. An event is a signal identified to be of Jovian origin whose amplitude is equal to or greater than three times the rms system noise in any given five minute interval measured from 0^h U.T.

2. A burst is a signal variation of Jovian origin of amplitude equal to or greater than three times the rms noise on a time scale of one second or longer.

An event therefore consists of a number of bursts.

†The NASA Jupiter conference at Goddard Space Flight Center in 1965 divided the System III longitudes into four regions: region D from 0° to 70°; region B 70°-190°; region A 190°-280°; region C 280°-360°. The main peak appears in region A, subsidiary peaks appear in regions B and C, and no peaks are found in region D.

central meridian longitude. Some polarization observations were carried out but they were not emphasized because of the more fundamental nature of the histogram and rotation period studies.

A partially polarized wave is completely specified by the total intensity I, the polarization fraction m, the axial ratio r, and the ellipse orientation x.[15] These quantities can be conviently represented in terms of the Stokes parameters which themselves are simply expressed in terms of circular components.[16] With oppositely polarized circular antennas the parameters I, m, r, and x may be obtained by measuring right and left circular intensities and the cross-correlation and phase difference between them. Early polarization experiments measured only right and left circular intensities so that the polarization was not completely known. In fact, to obtain an estimate of the axial ratio the wave had to be assumed to be completely polarized. In this case the axial ratio is given by[17]

$$r = \frac{L - R}{L + R} \qquad (1)$$

where L and R are the amplitudes of the left and right circular component signals respectively. Signals polarized right-handed in the radio sense* have $-1 \leq r < 0$ and signals polarized left-handed have $0 < r \leq 1$.

---

*A wave is right-handed polarized in the radio sense if the tip of the electric field vector rotates clockwise looking along the direction of propagation.

Up to 1961 all polarization measurements had been made close to 22 Mc/s,[7,18,19] except for a single observation at 19.6 Mc/s by Gardner and Shain.[20] Since observers in both hemispheres reported predominantly right-handed polarization, the effect was presumably not due to the Earth's ionosphere. Polarization measurements at 18.3 and 24.0 Mc/s were made in 1961 by Barrow.[21] Reporting a smaller proportion of right-handed polarization at 18.3 than at 24.0 Mc/s, he suggested that the gyrofrequency on Jupiter might be determined simply from changes in polarization mode at different frequencies and urged that observations be made at several different frequencies.

The following year Carr[22] and Barrow[23] observed a significant number of left-handed bursts at 16 Mc/s. Sherrill and Castles[24] reported varying proportions of left-handed bursts at frequencies from 15 to 24 Mc/s. Dowden's[25] observations at 10.1 Mc/s indicated that a higher proportion of left-handed bursts appeared to be associated with System III longitude regions B and C rather than with regions A and D. Observations described in Chapter IV tend to confirm these findings.

Up to this point axial ratios had been calculated on the assumption that the radiation is 100 per cent elliptically polarized. However, there are several other possibilities. For example, the radiation may consist of a pure circular component plus a random component.[26] Thus it becomes necessary to measure the random component to determine the degree of polarization and hence the axial

ratio. Dowden points out that this measurement is difficult to make, however, because Faraday rotation at decameter wavelengths is large and is both frequency and time dependent.*

An attempt to measure the random component was made in 1963 by Sherrill.[17,27] Using a system in principle similar to the Cornell University polarimeter,[28] Sherrill recorded right and left circular intensities and the cross-correlation product of their amplitudes. These measurements permit the calculation of polarization fraction and axial ratio. Sherill's results will be discussed in Chapters II, V, and VII.

The Florida State University Radio Observatory has recently set up a polarimeter system to measure all the parameters of polarization at 18 Mc/s. The overall time response of the system is considerably better than that of the system used by Sherrill. This results in better statistics for the number of bursts in an event since the possibility exists that Sherrill's low chart speeds and relatively long time constant (1.0 second) smoothed several bursts into one.

The amount of data obtained presents a formidable task in analysis. A typical Jupiter noise storm might produce 20 feet or more of record containing several hundreds of bursts. It will be the purpose

---

*Further discussion of this problem is deferred until Chapter II.

of this thesis to investigate possible compromise methods of record analysis and to compare preliminary results with those of other workers.

II. POLARIZATION MEASUREMENTS

A. Theory

According to theory,[15] partly polarized radio waves can be uniquely represented as the combination of a polarized part and an unpolarized part. The unpolarized component is specified by its intensity I_u. The polarized component is described by its intensity I_e, ellipse orientation χ and axial ratio r. The sense of rotation is indicated by the sign of r, as in Chapter I.

The four quantities I_u, I_e, χ, and r completely specify the wave. The wave may also be described by the Stokes parameters[15] which are given by:

$$\begin{aligned} I &= I_e + I_u \\ Q &= I_e \cos 2\beta \cdot \cos 2\chi \\ U &= I_e \cos 2\beta \cdot \sin 2\chi \\ V &= I_e \sin 2\beta \end{aligned} \qquad (2)$$

In terms of the Stokes parameters the polarization fraction $m = I_e/I$, axial ratio, orientation, and intensity may be found from:

$$\begin{aligned} I &= I \\ m &= (Q^2 + U^2 + V^2)^{1/2}/I \\ \sin 2\beta &= V/I_e, \quad r = \tan \beta \\ \tan 2\chi &= U/Q \end{aligned} \qquad (3)$$

The Stokes parameters have the advantage of being closely related to measurable quantities. In terms of circular components it can be shown that the Stokes parameters become:[16]

$$\begin{aligned} I &= I_R + I_L \\ Q &= 2RL\cos\gamma \qquad & I_R &= R^2 + I_u/2 \\ U &= 2RL\sin\gamma \qquad & I_L &= L^2 + I_u/2 \\ V &= I_L - I_R \end{aligned} \tag{4}$$

where L and R are the amplitudes of the left and right circular components of the polarized part of the wave. Fig. 2 shows the circular components of a polarized signal.

Using oppositely polarized circular antennas with an appropriate receiver and proper mixing circuitry, four outputs may be calibrated to read precisely I_L, I_R, the cross-correlation product $R \cdot L$, and the phase ϕ. With such a system the polarization parameters become:[28]

$$I = I_R + I_L$$

$$m = \frac{\left[(I_L - I_R)^2 + 4(R \cdot L)^2\right]^{1/2}}{I_R + I_L} \tag{5}$$

$$r = \tan\beta, \qquad \sin 2\beta = \frac{I_L - I_R}{\left[(I_L - I_R)^2 + 4(R \cdot L)^2\right]^{1/2}}$$

$$x = \phi/2.$$

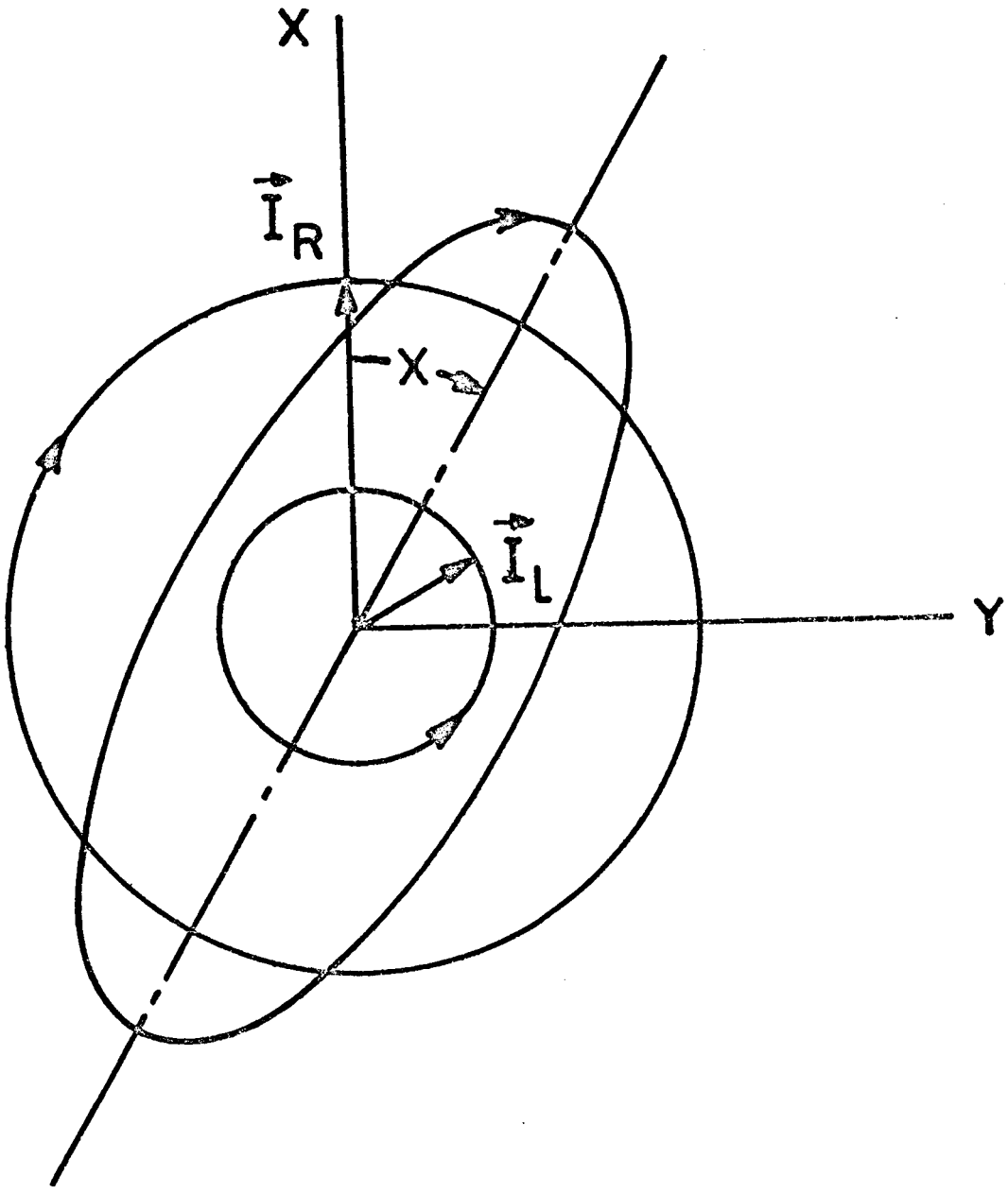

Fig. 2--Circular components of a right elliptically polarized wave oriented at an angle χ. The wave is propagating into the paper.

Measurement of the cross-correlation product in addition to the right and left circular intensities permits recognition of a number of different modes of polarization which would be indistinguishable if only right and left circular intensities were measured. For instance, random polarization and linear polarization look the same if the cross-correlation product is not measured. Similarly, pure elliptical polarization cannot be distinguished from the superposition of random and pure circular polarizations. Table 1 summarizes possible values of parameters of the wave for several types of polarization.

B. Faraday Rotation

In its passage through a homogeneous ionized medium in the presence of a magnetic field a partially polarized electromagnetic wave is split into two independent modes of propagation, each of which has a different phase velocity. If the frequency is sufficiently high, the two modes are circularly polarized with opposite senses of rotation unless the magnetic field is almost exactly transverse. The axial ratio and sense of rotation of the total wave are not altered but the polarization ellipse is rotated. The Faraday rotation of the polarization ellipse is given by[16]

$$\omega = (2.36 \times 10^{-3}) f^{-2} \int_0^z n B_z \, dz \qquad (6)$$

where ω is in radians, f is the frequency in megacycles, n is the number of electrons per cm^3, B_z is the longitudinal component of magnetic field

TABLE 1

POSSIBLE VALUES OF VARIOUS PARAMETERS
FOR SEVERAL TYPES OF POLARIZATIONS

Type of Polarization	$\|r\|$	m	I_R	I_L	R · L
Right-handed circular	1	1	I	0	0
Linear	0	1	I	I	I
Random	0	0	I	I	0
Random + Linear	0	$0<m<1$	I	I	$0<R \cdot L<I$
Right-handed elliptical	$0<\|r\|<1$	1	I	$0<I_L<I$	$0<R \cdot L<I$
Random + Right-handed circular	$0<\|r\|<1$	$0<m<1$	I	$0<I_L<I$	0
Random + Right-handed elliptical	$0<\|r\|<1$	$0<m<1$	I	$0<I_L<I$	$0<R \cdot L<I$

in gauss, and z is the path length in kilometers. Cohen[16] estimates that the Faraday rotation at 20 Mc/s is greater than 360 radians.

Ideally, any model for the origin of the Jovian decameter radiation should predict the electron density and magnetic field of the magnetosphere and the height of the source region. To be complete the model should also be able to predict the polarization of the radiation when it is emitted. Application of Equation 6 to the magnetoionic medium between the source region and the top of the Jovian magnetosphere should give the orientation of the polarization ellipse at the top of the magnetosphere. In principle, Equation 6 could also be used to find the Faraday rotation for the passage of the radiation through the interplanetary medium and the Earth's ionosphere. Also, in principle the ellipse orientation at the antenna can be calculated. These calculations might afford a check on the model. However, at the present time measurements of the ellipse orientation of the Jovian radiation are of little value since the magnetic field and the electron density in the interplanetary medium are not known with any certainty and the Faraday rotation due to the Earth's ionosphere can only be roughly estimated.

Measurements of the other polarization parameters should be more useful. These quantities measured at the antenna can be taken to describe the polarization at Jupiter if the dispersion due to Faraday rotation can be neglected. The effect of dispersion on an elliptically polarized noise signal distributed uniformly through a frequency

spectrum is to produce a continuum of polarization ellipses with a spread of orientations. Dispersion may arise either at the source or in the receiver. Dispersion at the source is due to the finite width of the source. Radiation from the bottom layer of the source suffers a Faraday rotation in its passage through the source. Thus each level of the source produces a different ellipse orientation so that at the top of the source the radiation appears to be partially polarized. This effect is small if the source region in the Jovian magnetosphere is small compared to the radius of the magnetosphere. In any case there is nothing that can be done about it since it is due entirely to the finite depth of the source.

Dispersion in the receiver is due to the finite bandwidth of the receiver. From Equation 6 the angular dispersion rate is

$$\frac{d\omega}{df} = -2\frac{\omega}{f} \text{ radians/cycle.} \qquad (7)$$

If the bandwidth is small compared to the center frequency, then

$$\frac{\theta}{\omega} \simeq 2\frac{\Delta f}{f} \qquad (8)$$

where θ is the dispersion in radians in the frequency band between f_1 and f_2 and $\Delta f = f_2 - f_1$.

According to Cohen[16], the dispersion may be significant whenever the product of Faraday rotation and relative receiver bandwidth is greater than half a radian for then $\theta \geq 1$ radian by Equation 8. Applying Equation 8 to the 18 Mc/s polarimeter at Florida State University using a bandwidth of 3.5 kc/s and Cohen's estimate of Faraday rotation at

20 Mc/s, the Faraday dispersion is found to be about .17 radians. This is comfortably within the limit specified by Cohen, so that dispersion in the receiver is probably not significant.

It should be noted that Cohen's analysis assumes that the radiation is incident vertically, that is, that the zenith angle i is zero. The effect of a changing zenith angle may be accounted for by multiplying the right hand side of Equation 8 by sec i. It is easily seen that the zenith angle would have to be quite large for the dispersion in the receiver to be significant.

The dispersion in the receiver could be decreased by reducing the bandwidth of the receiver, but this affects the relative power of the receiver noise fluctuations according to

$$\frac{\Delta p}{p} = \frac{1}{\sqrt{(T \Delta f)}} \qquad (9)$$

where T is the time constant of the receiver. Thus to decrease the bandwidth of the receiver is to decrease the signal-to-noise ratio. A compromise value must therefore be adopted.

C. Theories on the Jovian Decametric Radiation

Present theoretical considerations of the decameter radiation from Jupiter favor two models. The theory of Warwick[11, 29] suggests that forward-beamed Cerenkov radiation emitted at a frequency just below the plasma cyclotron frequency by particles precipitated from the Jovian Van Allen belts can explain the spectral data obtained with the

High Altitude Observatory 7.5-41 Mc/s swept-frequency solar spectrograph. The radiation escapes after reflection either within dense layers of the Jovian ionosphere or at the surface of the planet. The radiation is only observed at the Earth for certain orientations of the assumed dipolar magnetic field and the planet's surface.

After trial and error Warwick found that the characteristic longitude profile and frequency drifts above 20 Mc/s can be explained by assuming the dipole to be inclined 9° to the rotational axis and located well to the south of the equatorial plane. This result is subject to the restrictions that the electrons are precipitated from the main radiation belt at two or three Jupiter radii from the surface and that the radiation is confined to within $\pm$ 10° of the field lines.

According to Ellis[30], there are several difficulties in Warwick's theory, not the least of which is the requirement of a highly asymmetric dipole location, although this is substantiated to some extent by the observations of Morris and Berge[31]. Later observations by Berge[32], however, do not indicate that the field configurations required by either Warwick's theory or the Ellis and McCullough theory are present, although a small asymmetry is not ruled out. Also Cerenkov radiation in general is not emitted in the direction of particle motion. Since the radiation is generated with a frequency just below the plasma cyclotron frequency, the decrease in magnetic field as the radiation travels outward means it will have to pass through a magnetoionic stop region where the

wave frequency is equal to the cyclotron frequency. It is difficult to see how high attenuation can be avoided, since this region must not be very far above the generating region.

The Doppler-shifted cyclotron theory of Ellis and McCullough[30, 33] is perhaps more plausible as it seeks to explain the Jovian radiation in terms of known terrestrial magnetospheric processes. The theory also makes predictions about the polarization of the radiation that can be tested experimentally.

Ellis and McCullough point out that the radiation, either Cerenkov or cyclotron emission, must pass through a region of imaginary index of refraction if it is to escape. However, the dependence of the refractive index on frequency permits the forward-beamed radiation in the extraordinary mode to escape the source region, if it is Doppler-shifted to a frequency for which the index of refraction is real.

The origin of the radiation is assumed to be cyclotron emission from magnetically disturbed electron streams near the boundary of the Jovian exosphere at high magnetic latitudes. After refraction the emerging radiation is mainly confined to the surface of a cone whose axis is the magnetic field line. The angular radius of the cone is given by Snell's law

$$\sin \alpha_m = n \cdot \sin \delta \qquad (10)$$

where δ is the angle between the wave normal and the magnetic field

vector and n is the index of refraction. The axial ratio is given by

$$r = \pm \cos \alpha_m . \tag{11}$$

Fig. 3 shows the predicted distribution of axial ratios.[33] Since the cone angle α_m depends strongly on the pitch angle of the electrons, the peak of the distribution may be changed considerably by a small change in the magnetic latitude of the source region.

It can also be shown from the theory that the summed axial ratio and the integrated power W are related to the number of bursts N by

$$\Sigma | r | \propto N^p \tag{12}$$

$$W \propto N^q \tag{13}$$

where p = 1.05 and q = 1.3 from the initial assumption of the theory.

Dowden found that observations at 10.1 Mc/s gave an axial ratio distribution similar in shape to the theoretical curve in Fig. 3, if it is assumed that apparent axial ratios below 0.2 are produced by superposition of bursts with higher axial ratios but opposite senses of polarization.

Fig. 4 shows the axial ratio distributions at 10.1 Mc/s and also axial ratio distributions at 16 and 18 Mc/s observed by Barrow.[34]

Dowden's observations also give a value of 1.10 for p in Equation 12 and a value of 1.51 for q in Equation 13. The former value is in good agreement with the predicted value. The discrepancy in the

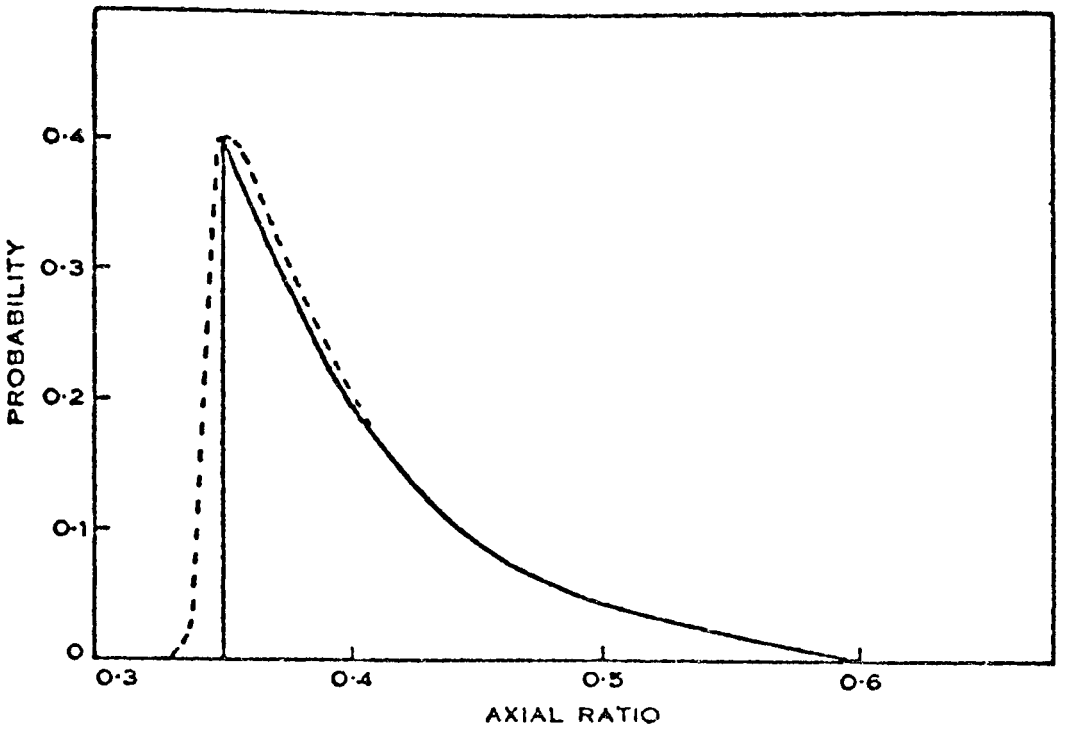

Fig. 3--Distribution of axial ratios according to the Ellis and McCullough theory.

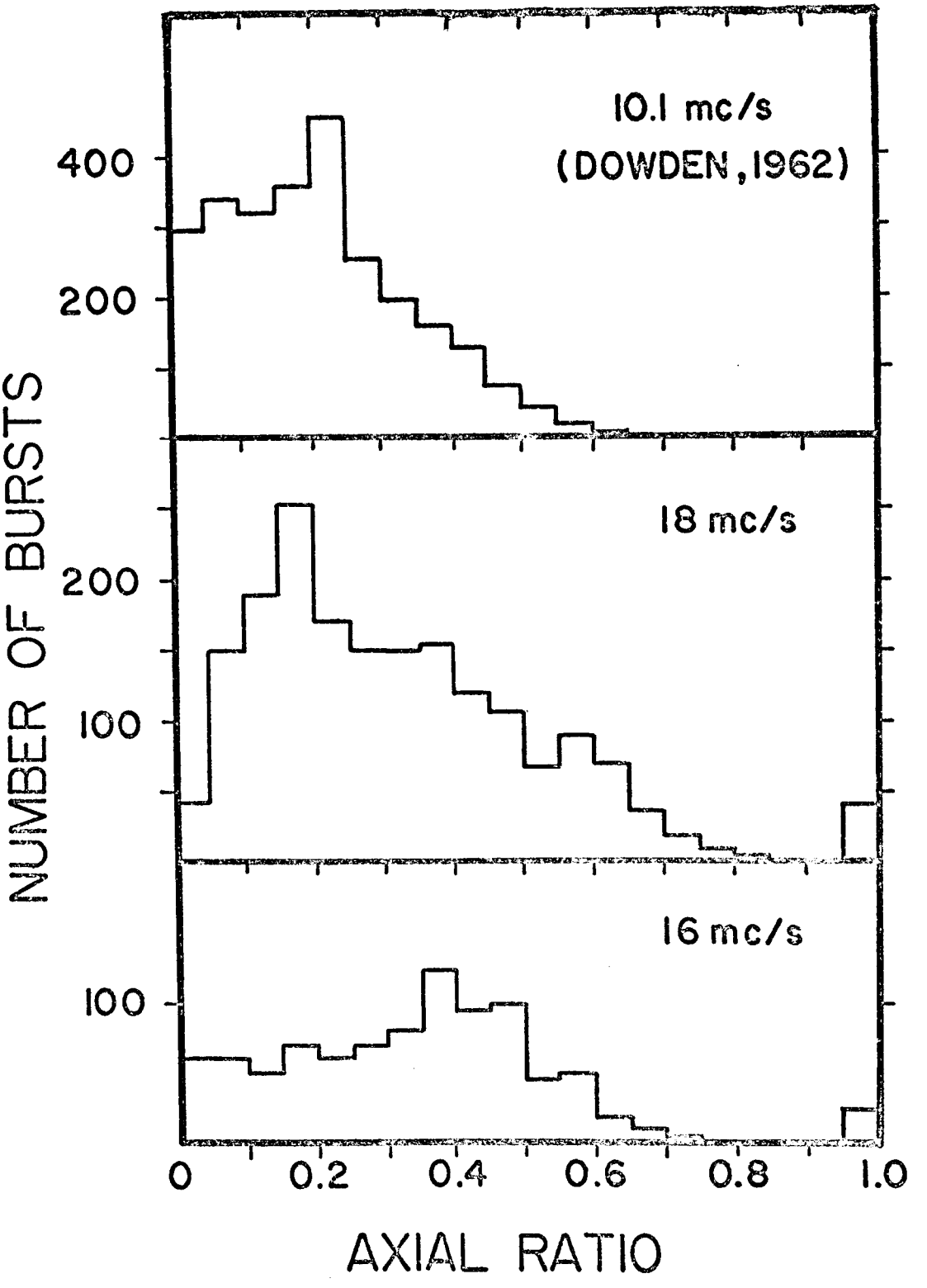

Fig. 4--Axial ratio distributions at 10.1, 16, and 18 Mc/s.

latter value could be accounted for by failing to allow for superposition of bursts.

Sherrill assumed $p = 1.05$ in Equation 12 and fitted this slope to his observations. However, his measurements gave axial ratio distributions which were peaked around 0.8 instead of at 0.3 as Fig. 3 predicts. According to Ellis[30], this can be accounted for by assuming that the radiation is emitted at magnetic latitudes near 68° instead of between 75 and 80° as originally supposed.

One interesting feature of the Ellis and McCullough theory is the use of a magnetic dip anomaly to explain the observed longitude profiles. The magnetic dip anomaly is a well-known terrestrial phenomenon and the proposed anomalies do not appear to be excessive when compared with the terrestrial ones.

Another attractive feature of the theory is the possibility of an explanation of the observed dependence of the radiation on the orbital position of the satellite Io. Modifications of either electron streams in the Jovian magnetosphere or the momentum distribution of electrons within the streams may be caused by hydromagnetic or electromagnetic radiation from Io. Observations of the terrestrial magnetosphere have shown that such radiation can stimulate emission of coherent radiation by a non-radiating particle stream.

The theory has some difficulties when compared with other features of the earth's magnetosphere. For instance, the scale height

of 2000 km found from predicted electron densities implies electron temperatures of 7500 degrees Kelvin in the lower Jovian magnetosphere as compared to 1000 to 2000 degrees Kelvin for the Earth.

The Ellis and McCullough theory is by far the most fully developed of the theories of the decameter radiation. It appears to be the most attractive because of its use of mechanisms which are known to apply to the terrestrial magnetosphere.

III. THE 18 MC/S POLARIMETER

A. Instrumentation

The antenna used for the 18 Mc/s polarimeter observations and its polar diagram are shown in Fig. 5. The antenna consists of two crossed five-element Yagi antennas alt-azimuthally mounted on a 35 foot tower. The mounting permits up to eight hours of observation per night. According to the manufacturer's specifications the gain of the antenna is about 12.5 db for each polarization, probably an optimistic estimate. A more realistic figure is about 10.5 db with respect to a half-wave dipole.

The antennas were fed through approximately 150 feet of RG-14AU transmission line (z_o = 50 ohms) to a conventional hybrid ring[35] to simulate left and right circular components as shown in Fig. 6. These components were fed to a rack panel where receiver or calibrator connections could be made.

The RF outputs from the rack panel were fed to the polarimeter receiver.* Fig. 7 shows a schematic of the receiver. Receiver characteristics are listed in Table 2. An external noise source and a vacuum tube voltmeter were used to balance the gains of the left and

*Made to specifications by Aerospace Research, Inc.

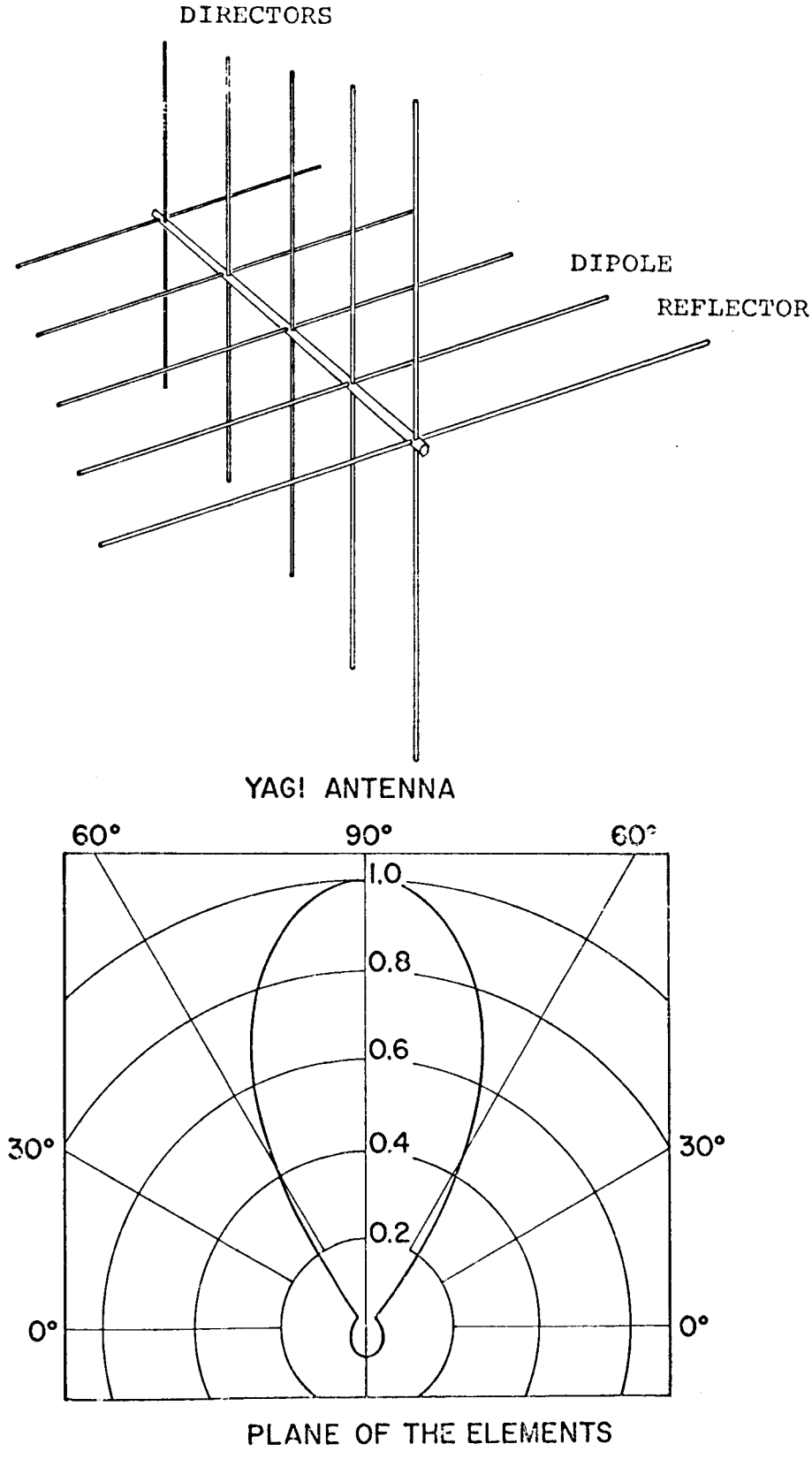

Fig. 5--The crossed-Yagi antenna and its reception pattern for one polarization.

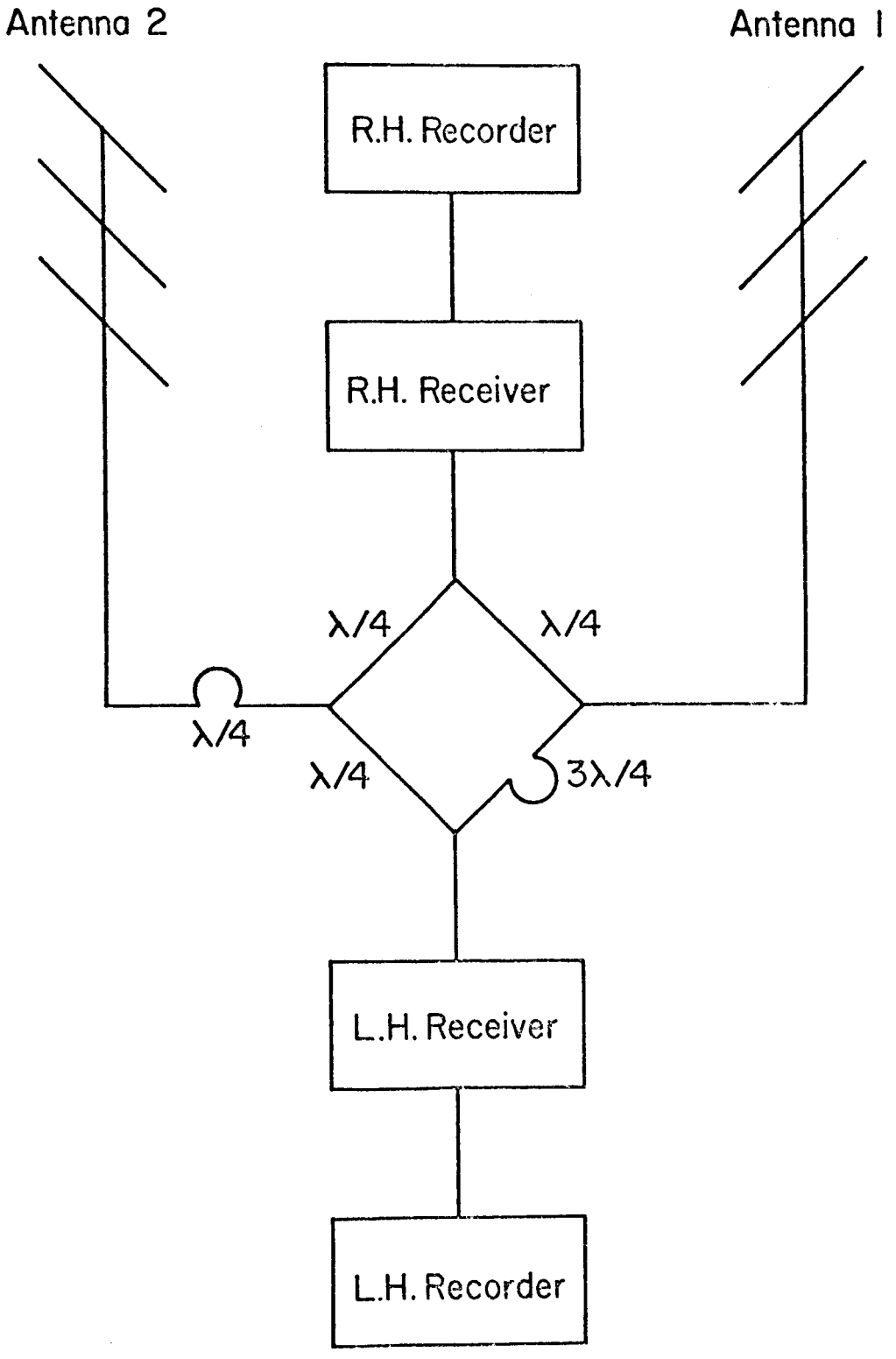

Fig. 6--Schematic of the 18 Mc/s polarimeter system showing the hybrid ring circuit.

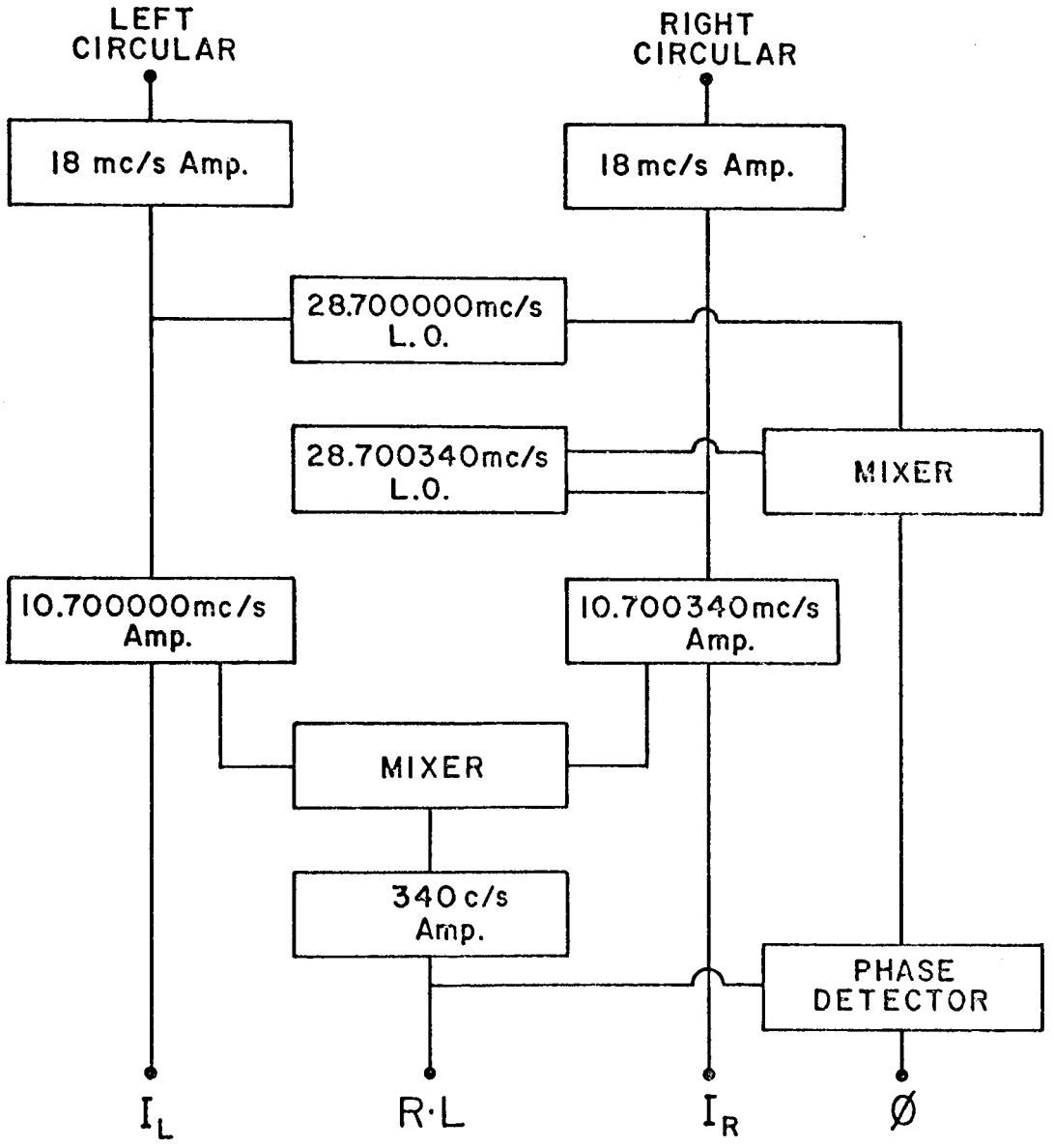

Fig. 7--Schematic of the 18 Mc/s polarimeter receiver.

right hand sensitive channels, I_L and I_R in Fig. 7, before each observing period.

TABLE 2

RECEIVER CHARACTERISTICS

Input impedance[a]	75 ohms
Center frequency	18 Mc/s
Manual tuning	± 1/2% of center frequency
Electronic sweep tuning	± 1/2% of center frequency
Noise figure	6 db
IF frequency	10.7 Mc/s
IF bandwidth	3.5 or 15 kc/s, selectable
Time constant	0.1 or 1.0 second, selectable
Audio frequency amplifier bandwidth	18 c/s

[a]Changed to 50 ohms for 1966-1967 observations

Signals from local oscillators at 28.700000 and 28.700340 Mc/s are mixed with the RF signal after amplification to produce the IFs of 10.700000 and 10.700340 Mc/s. The signals pass through selectable 3.5 or 15 kc/s bandwidth filters at the IF amplifiers. Part of the outputs from each of the IF amplifiers are fed to a single product detector whose output is proportional to the product of the amplitudes of the I_L and I_R channels, if the signals are coherent. This produces the cross-correlation or correlator channel shown as the R • L channel in Fig. 7. The output of the R • L channel is fed to a phase detector which produces

a DC voltage proportional to the phase difference of the I_R and I_L signals. This is the ϕ channel in Fig. 7.

The four outputs from the receiver were fed to a Sanborn four channel DC thermal writing amplifier-recorder system capable of chart speed from 0.25 mm/sec to 100 mm/sec. The zero position was adjusted if necessary before the observation period to obtain a convenient background level. Observations were made with a chart speed of 2.5 or 5 mm/sec, a time constant of 0.1 second, and a bandwidth of 3.5 kc/s.

B. Calibration

Two distinct calibration processes were necessary for the 18 Mc/s polarimeter. The instrumental calibration was carried out before and during the watch to insure that the I_R and I_L channels were gain matched. An external noise source was connected to the antenna inputs and the gain of the I_L channel was matched to that of the I_R channel. This had to be checked at the start of each watch as the match was unstable over periods longer than several hours. The stability was improved considerably by leaving the equipment turned on between observations.

A schematic of the polarization calibration system is shown in Fig. 8. The outputs of the noise sources are fed to the antenna input terminals of the receiver. Two independent crystal diode noise sources were used to simulate the unpolarized background radiation. The output

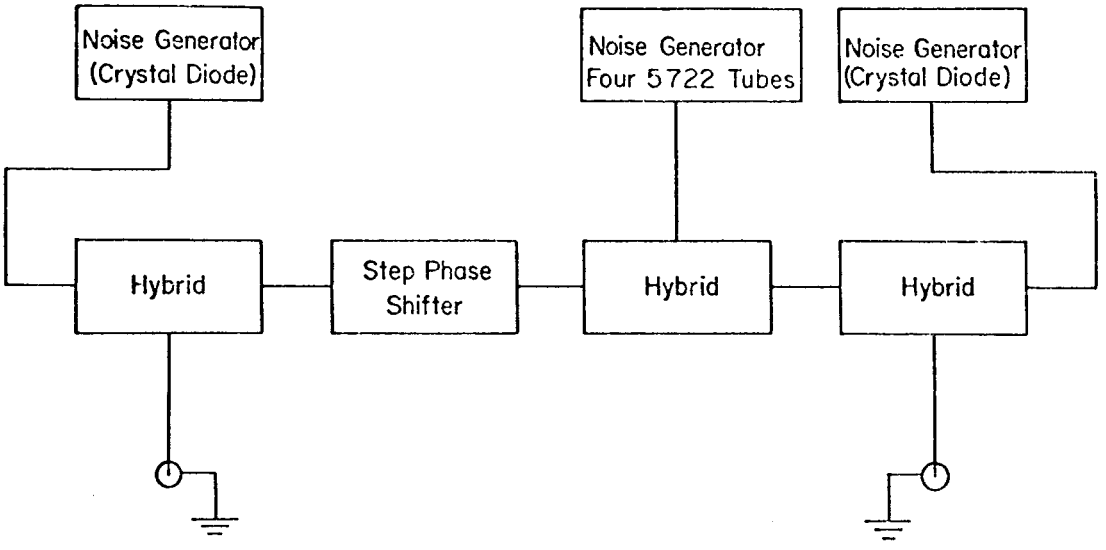

Fig. 8--Schematic of the 18 Mc/s polarimeter calibration system.

of a temperature saturated diode noise generator was divided equally by a commercial transformer hybrid to provide a coherent noise source which simulated completely polarized signals. The attenuator could be placed in either side of the circuit to simulate various polarizations. Various cable lengths connected to a coaxial switch could replace the attenuator in the circuit. This also simulated various polarizations and phase differences. The tube noise generator was fixed to generate a given current and the corresponding deflection above background was recorded on the Sanborn recorder. This was done for a series of current values.

A temperature saturated diode produces in the receiver a noise current i_n, the mean square value of which, in the frequency bandwidth Δf, is given by[36]

$$i_n^2 = 2eI\Delta f \tag{14}$$

where I is the diode current and e is electronic change. The power available from the diode is given by

$$P = \left(\frac{i_n}{2}\right)^2 R = \frac{e}{2} IR\Delta f \tag{15}$$

in terms of the current in the diode and the load impedance R.

The recorder deflection D above the background level is directly proportional to the output current of the detectors. The output current of the detectors is proportional to some power t of the current i_n.

Therefore

$$i_n^t \propto i_{out} \propto D. \tag{16}$$

Combining Equations 15 and 16

$$P^{1/2} \propto I^{1/2} \propto i_n \propto D^{1/t}. \tag{17}$$

It is easily seen that the relation between tube current I and recorder deflection D will have the form

$$I = kD^{2/t} \tag{18}$$

where t is the detector law and k is some constant. If the curve is plotted on log-log graph paper, it has the form

$$\log I = \frac{2}{t} \cdot \log(D) + \log(k). \tag{19}$$

Thus a Jupiter burst which produces a recorder deflection D may be related to a tube current I by Equation 19.

The advantage of this method is that t and k need not be known. A current corresponding to a particular deflection may simply be read off the log-log plot. For more precise calculations, however, the calibration curves may be constructed by the method of least squares using the calibration points obtained at the end of each event. A typical set of calibration curves is shown in Fig. 9 for the third event of January 28, 1966. The curve labelled A is tube current versus right hand channel recorder deflection; the B curve is current versus left hand channel deflection; The C curve is current versus correlator

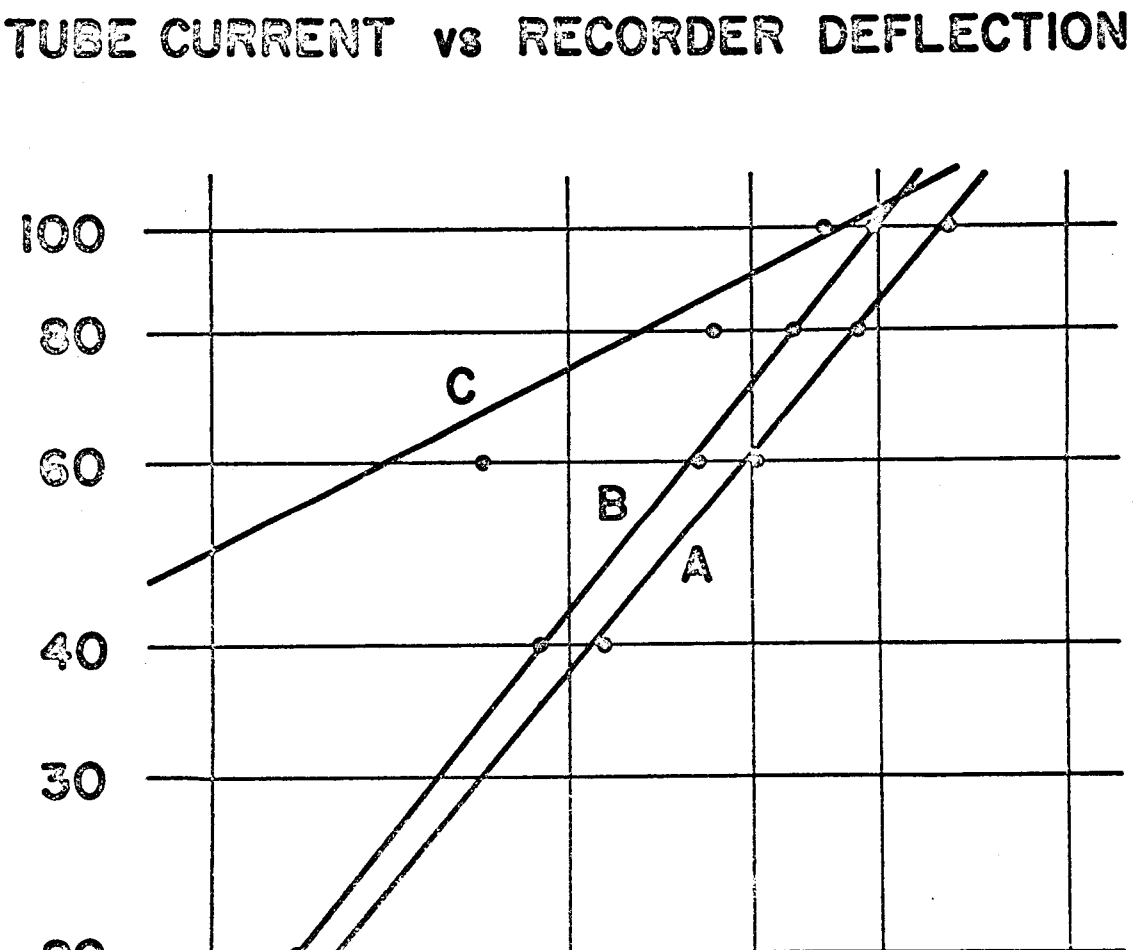

Fig. 9--Calibration curves for the event of January 28, 1966.

channel deflection. Fig. 10 shows the calibration of the record from which these curves were constructed.

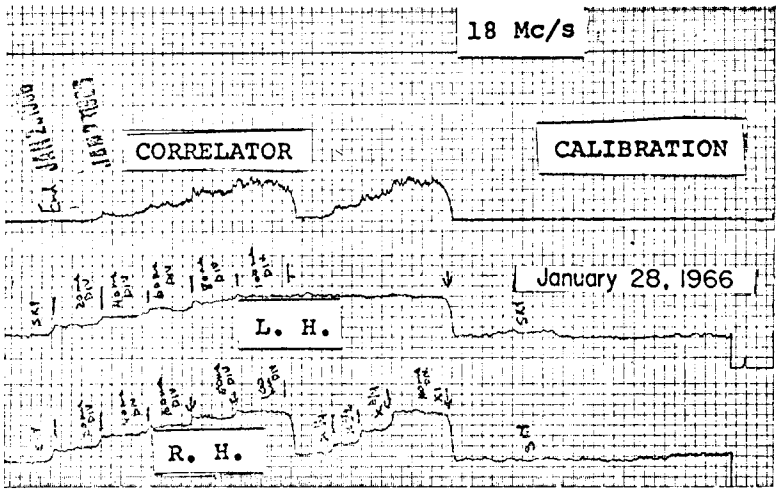

Fig. 10--Calibration of the January 28th record of Jupiter activity.

IV. OBSERVATIONS

Polarization observations were made at Florida State University during the 1965-1966 apparition of Jupiter at 12.5, 16, 18, and 22 Mc/s. In addition to the measurement of the four Stokes parameters at 18 Mc/s the right and left circular components at 18 Mc/s were also recorded separately as part of the program of study of the Jovian I-pulses. Measurements of the right and left circular components of polarization were made at 12.5, 16, and 22 Mc/s.

The polarimeter system for the measurement of the Stokes parameters had been described in Chapter III. The antenna-receiver-recorder systems at the other frequencies have been described by Lee[37]. Table 3 lists the periods during which the various frequencies were monitored.

TABLE 3

OBSERVATION PERIODS FOR VARIOUS FREQUENCIES

Frequency	Period of Observation
12.5 Mc/s	February 12, 1966 to March 17, 1966
16 Mc/s	November 21, 1965 to March 17, 1966
18 Mc/s	December 6, 1965 to March 17, 1966
22 Mc/s	November 21, 1966 to February 4, 1966

Smoothed histograms of the polarization observations at 16, 18, and 22 Mc/s are shown in Fig. 11. The right hand histograms contain all activity recorded on the right hand channels; the left hand histograms contain all activity recorded on the left hand channels.

The most striking feature of these histograms is the difference between the relative height of the peak in region A in the left and right hand histograms. In the right hand histograms it is by far the highest but in the left hand histograms it is about the same as the other peaks. Another interesting feature is the similarity of the left hand histograms, particularly the 16 Mc/s histogram, to the I-pulse histogram[9,37] shown in Fig. 12. The I-pulse histogram was constructed from 1965-1966 observations at Florida State. It contains only periods of activity during which I-pulses were recorded.

Measurement of the Stokes parameters began December 6, 1965. Unfortunately the final calibration procedure was not fully established until late January, 1966. As a result only five events recorded under suitable observing conditions have good calibrations. These are listed in Table 4. Analysis of these events is carried out in Chapter V. The events in Table 4 were all recorded with a time constant of 0.1 second and a receiver bandwidth of 3.5 kc/s. The chart speed for the January 28th event was 2.5 mm/sec; for the other events the chart speed was 5 mm/sec.

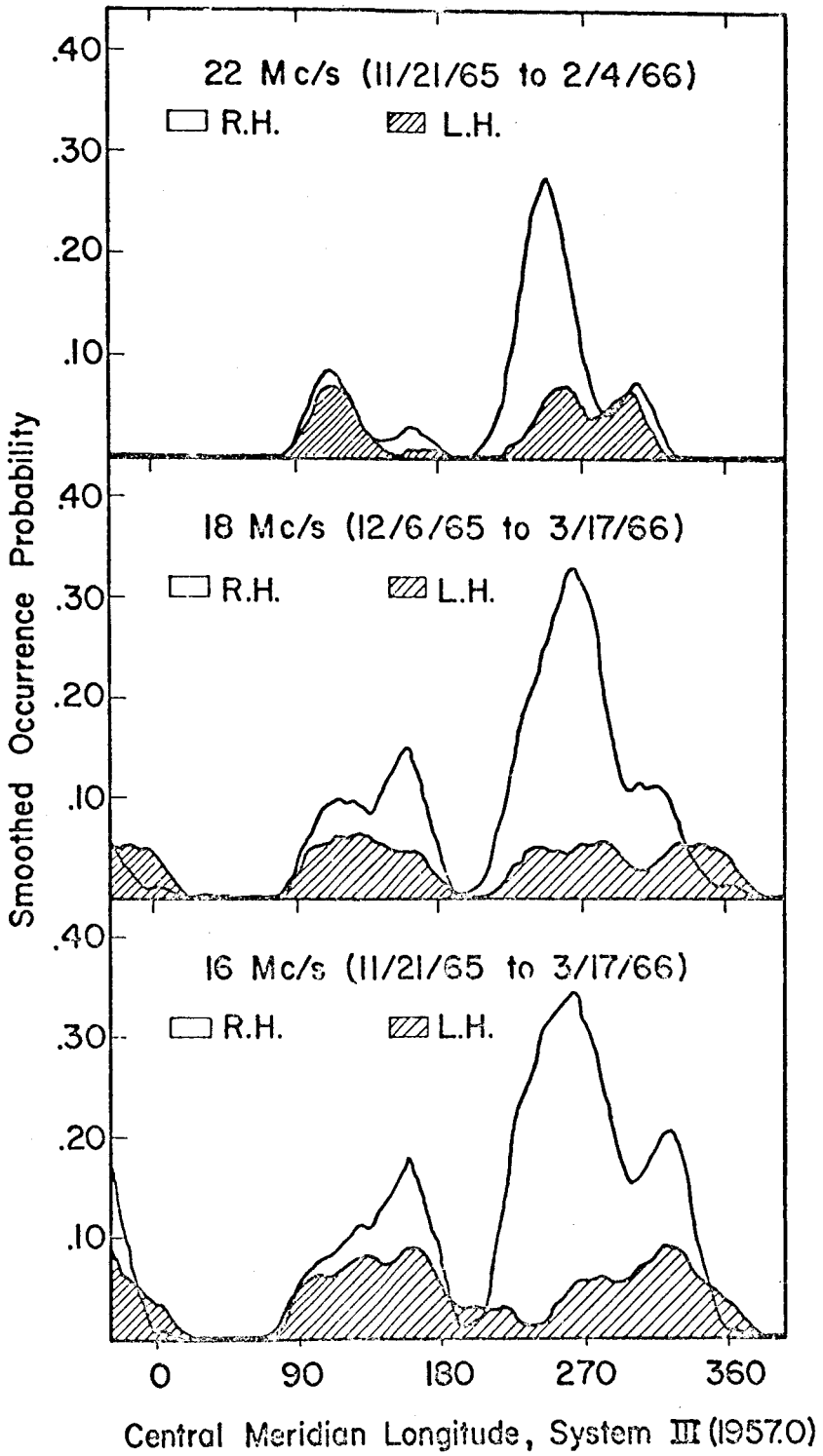

Fig. 11--Histograms of polarization observations 1965-66.

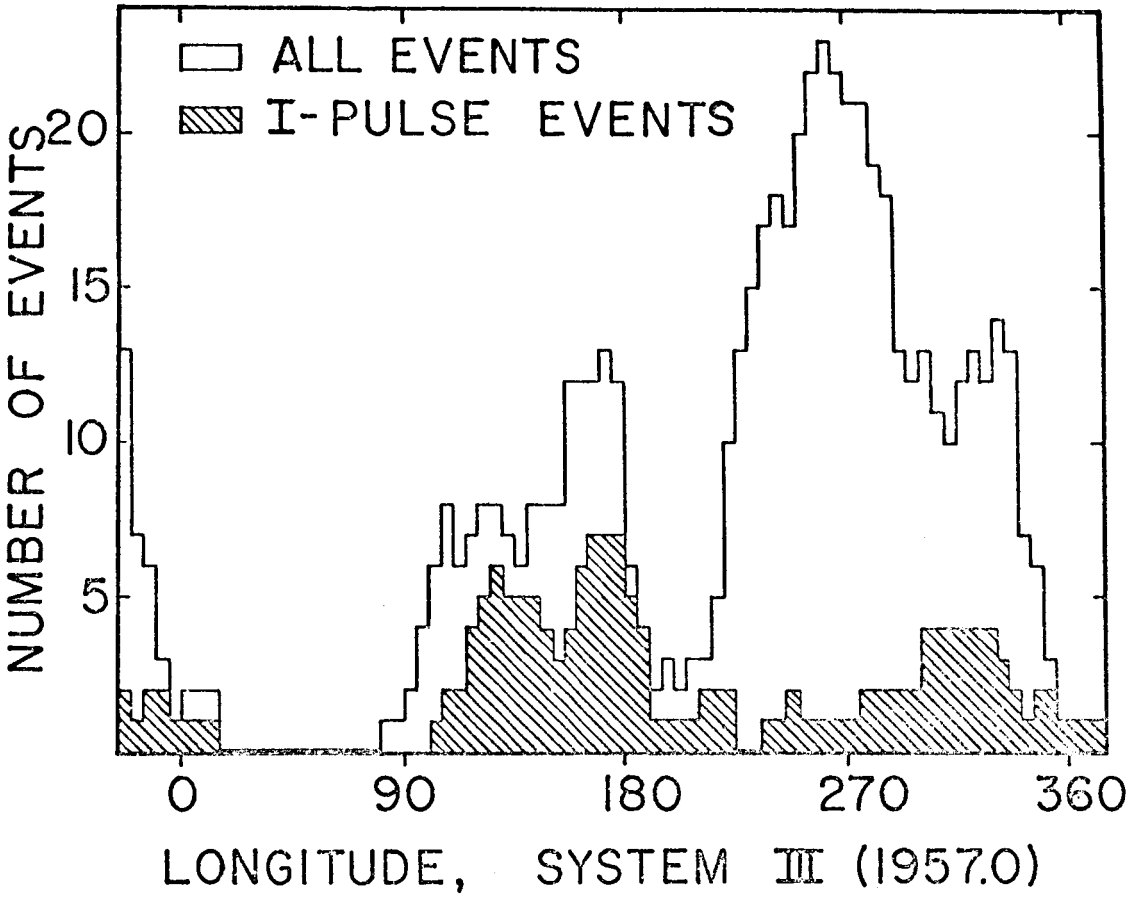

Fig. 12--Histogram of I-pulse activity 1965-66.

The event of January 28th was the third event recorded that night. The first event at around 0300 U. T. was predominantly right-handed with a small amount of weak left-handed activity. A portion of this event is shown in Fig. 13a. This event is not included in Table 4 because the chart speed was 1 mm/sec and the time constant was 1.0 second.

TABLE 4

JUPITER EVENTS WHICH HAVE GOOD CALIBRATIONS

Date	Universal Time	System III Longitude	Position
January 28, 1966	0539-0559	0-11	245-248
February 23, 1966	0148-0157	173-178	262-263
March 2, 1966	0138-0235	140-180	85-95
March 16, 1966	0342-0422	160-185	70-76
March 17, 1966	0153-0204	245-251	258-260

The second event of January 28th occurred near 0430 U. T. and consisted entirely of widely separated and weak right-handed bursts. It is interesting to note that at this time a strong I-pulse event was being recorded at 14 and 16 Mc/s.

The I-pulse event at 14 Mc/s appeared to continue well past the beginning of the third event at 18 Mc/s event though by this time Jupiter was well beyond the half-power points of the beam pattern of the 14 Mc/s array. At 18 Mc/s the event was predominantly left-handed

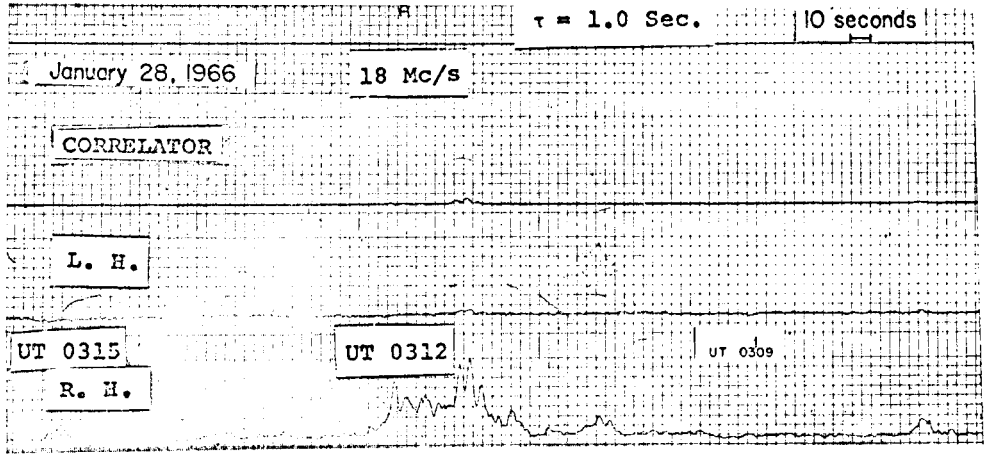

Fig. 13a--A portion of the January 28th record.

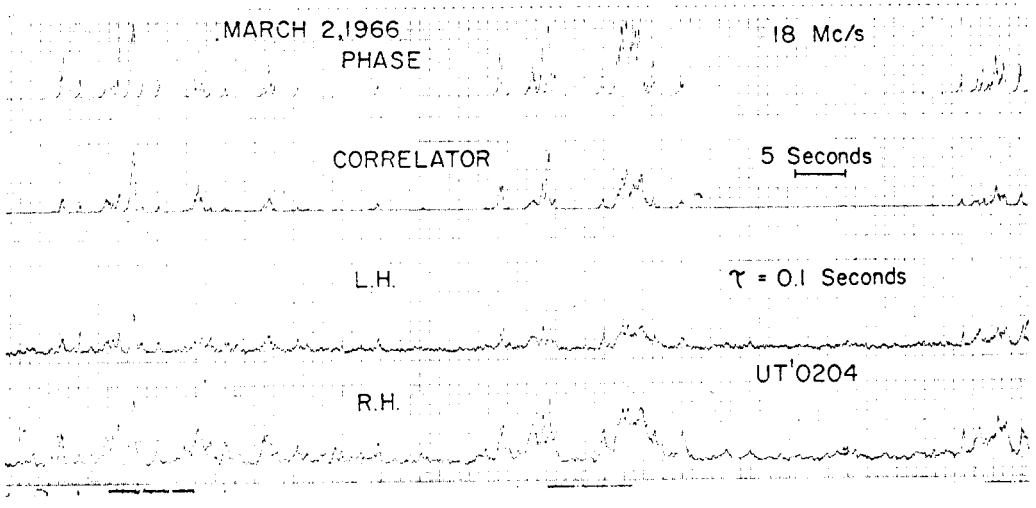

Fig. 13b--A portion of the March 2nd record.

throughout; at the beginning there was considerable strongly correlated right-handed activity, shown in Fig. 14a. Fig. 14b shows the right-handed activity having died away nearly completely within a few minutes.

Predominantly left-handed activity was recorded again on February 23rd. Part of this event is shown in Fig. 15b. Earlier on this date, around 0100 U.T., a weak, completely left-handed event was recorded and is shown in Fig. 15a.

The events of March 2nd, 16th, and 17th were all predominantly right-handed events. Fig. 13b shows a segment of the March 2nd record and is typical of all three events. There were some weak uncorrelated left-handed bursts mixed in with the right-handed activity on March 2nd.

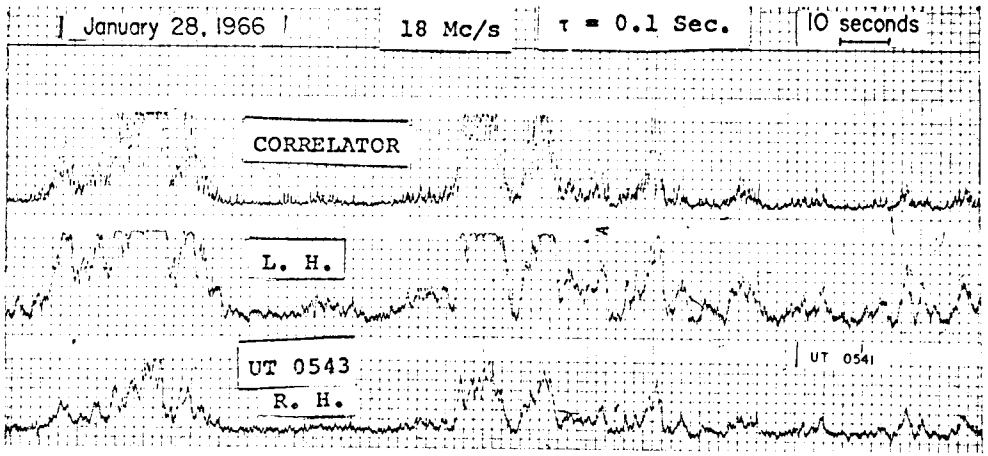

Fig. 14a--A portion of the January 28th record.

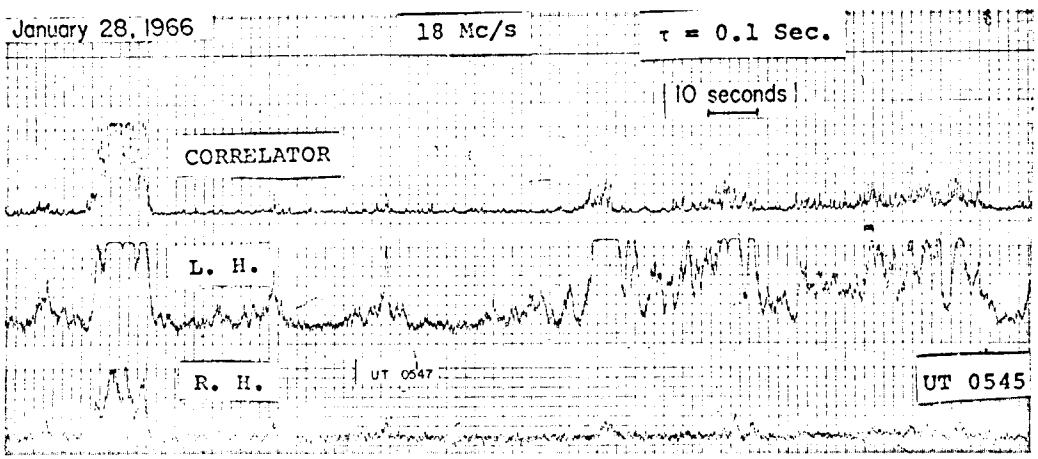

Fig. 14b--A portion of the January 28th record.

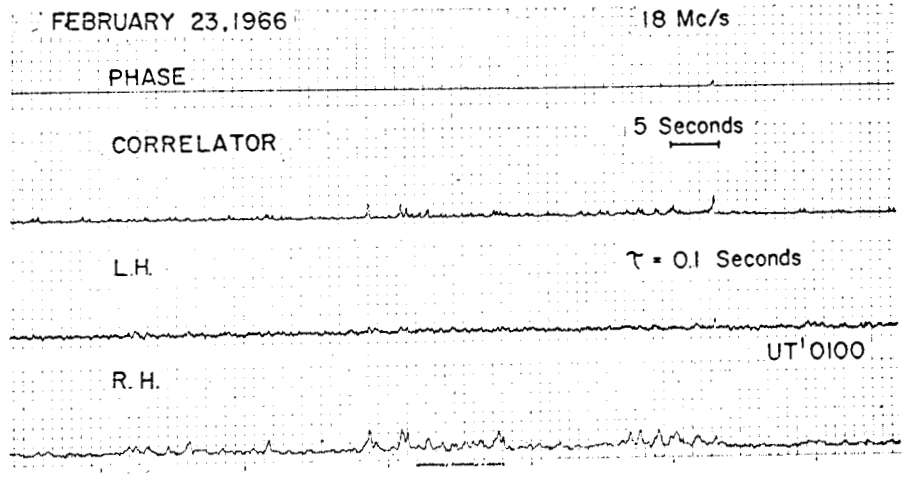

Fig. 15a--A portion of the February 23rd record.

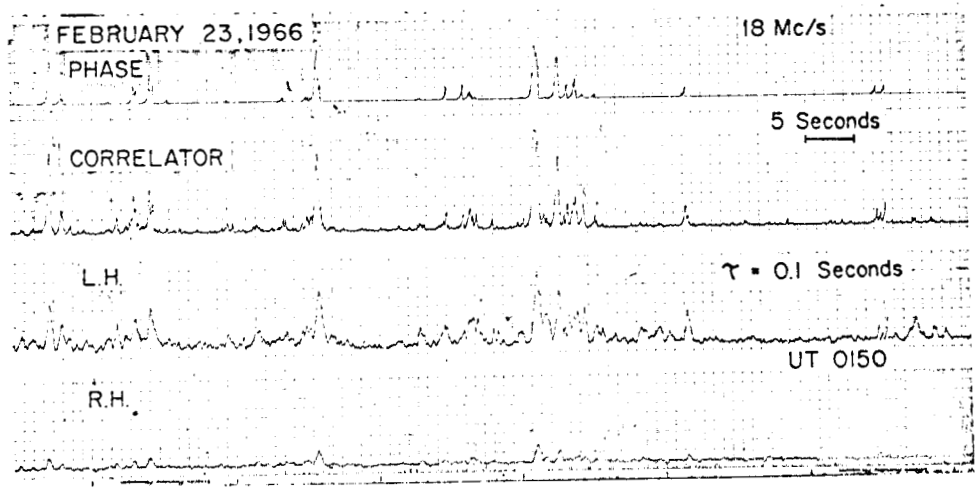

Fig. 15b--A portion of the February 23rd record.

V. ANALYSIS OF RECORDS

Discussion of earlier polarization observations (Dowden at 10.1 Mc/s, Sherrill at frequencies between 15 and 24 Mc/s, and Barrow at 16 and 18 Mc/s) must include consideration of the overall time characteristics of the respective polarimeter systems. The observations reported by Dowden consisted of 35 mm film of two parameters of polarization taken at six inches per hour. Sherrill's observations were made with a time constant of 1.0 second and a recorder speed of 0.2 mm/sec. Barrow's recorder speed was 2 mm/sec with a time constant of about 0.1 second, but he too recorded only two parameters of polarization.

The effect of recording speeds like those used by Dowden and Sherrill is to compress small time intervals into small distances on the record of the event. Thus at 0.2 mm/sec one millimeter equals five seconds. The segments of records shown in Figs. 13-15 contain several groups of three or more bursts occurring within a five second interval. It would be difficult to resolve these bursts using a chart speed of 0.2 mm/sec, even with a time constant as short as 0.1 second.

The possibility of superposition of bursts in Dowden's and Sherrill's records could introduce errors in the assessment of burst characteristics. For example, a comparison of the dependence of

summed axial ratio and integrated power on number of bursts as predicted by the Ellis and McCullough theory with the observed dependence could contain systematic counting errors.

The chart speeds of the Jupiter events listed in Table 4, together with the receiver time constant of 0.1 second, permitted the resolution of adjacent bursts if their peaks were separated by 0.4 second. The improved burst resolution reduces considerably the probability that several bursts may be superposed, if the bursts are not I-pulses. Thus great improvement of the statistics for an individual event is possible.

However, an increase in number of bursts per event produces a corresponding increase in time required for analysis of the event. Tables 4 and 5 show that a large number of bursts may occur in a period of a few minutes. A method of analysis of the records which reduces the number of data points per event yet retains the main features of a burst analysis would permit more rapid analysis of large numbers of Jupiter events. This method would results in an artificial superposition of bursts, but the time characteristics of the polarimeter system would permit the improvement of statistics if so desired.

Development of such a method necessarily entails analysis of some records at short time intervals to provide a standard of comparison. This has been done for each event listed in Table 5. The interval chosen was 0.4 second, or one millimeter on the record of the January

28th event and two millimeters on the records of the other events. Axial ratio and polarization fraction were computed according to Equations 5 for each point whose deflection on either the I_L or the I_R channel was greater than the larger of five millimeters or three times the rms system noise criterion mentioned in Chapter I. The three times rms system noise criterion was a weaker restriction for all the events except that of January 28th. The five millimeter restriction was imposed since the error analysis of Chapter VI showed that calculation for points with deflections on both the circular component channels less than five millimeters above the background level could be highly inaccurate. Block diagrams of the distribution of values of axial ratio and polarization fraction were then compiled for the complete set of points in this analysis.

TABLE 5

NUMBER OF POINTS IN EACH ANALYSIS OF EACH EVENT

Event	Burst	0.4 Sec.	2.0 Sec.	6.0 Sec.
January 28, 1966	256	1376	347	139
February 23, 1966	169	249	99	41
March 2, 1966	1011	1836	642	309
March 16, 1966	184	256	105	58
March 17, 1966	294	301	109	50

A less detailed analysis was made by selecting in each 2.0 second interval the point with the largest deflection on either of the circular component channels. The selection was made from the set of points comprising the 0.4 second analysis and was also subject to the minimum deflection above background level criterion discussed above. Calculation of polarization fraction and axial ratio for each point thus obtained permitted the construction of block diagrams of the distribution of values of these quantities for this set of data points. Similarly, distributions of axial ratio and polarization fraction were obtained using 6.0 second intervals.

Finally, axial ratio and polarization fraction were computed for the peak of each burst, again subject to the requirement that each peak be at least five millimeters or three times the rms system noise above the background level on either of the circular component channels. Two bursts were considered to be resolved if their peaks were separated by 0.4 second or more. Block diagrams of the distribution of values of axial ratio and polarization fraction were drawn for this set of points.

Figs. 16-20 compare the four distributions for each event. Reading from the top downward, the distributions are for the burst peak, 0.4 second, 2.0 second, and 6.0 second analyses respectively. Each distribution is plotted for 0.1 intervals of axial ratio r and polarization fraction m and has been normalized by dividing the number of points in

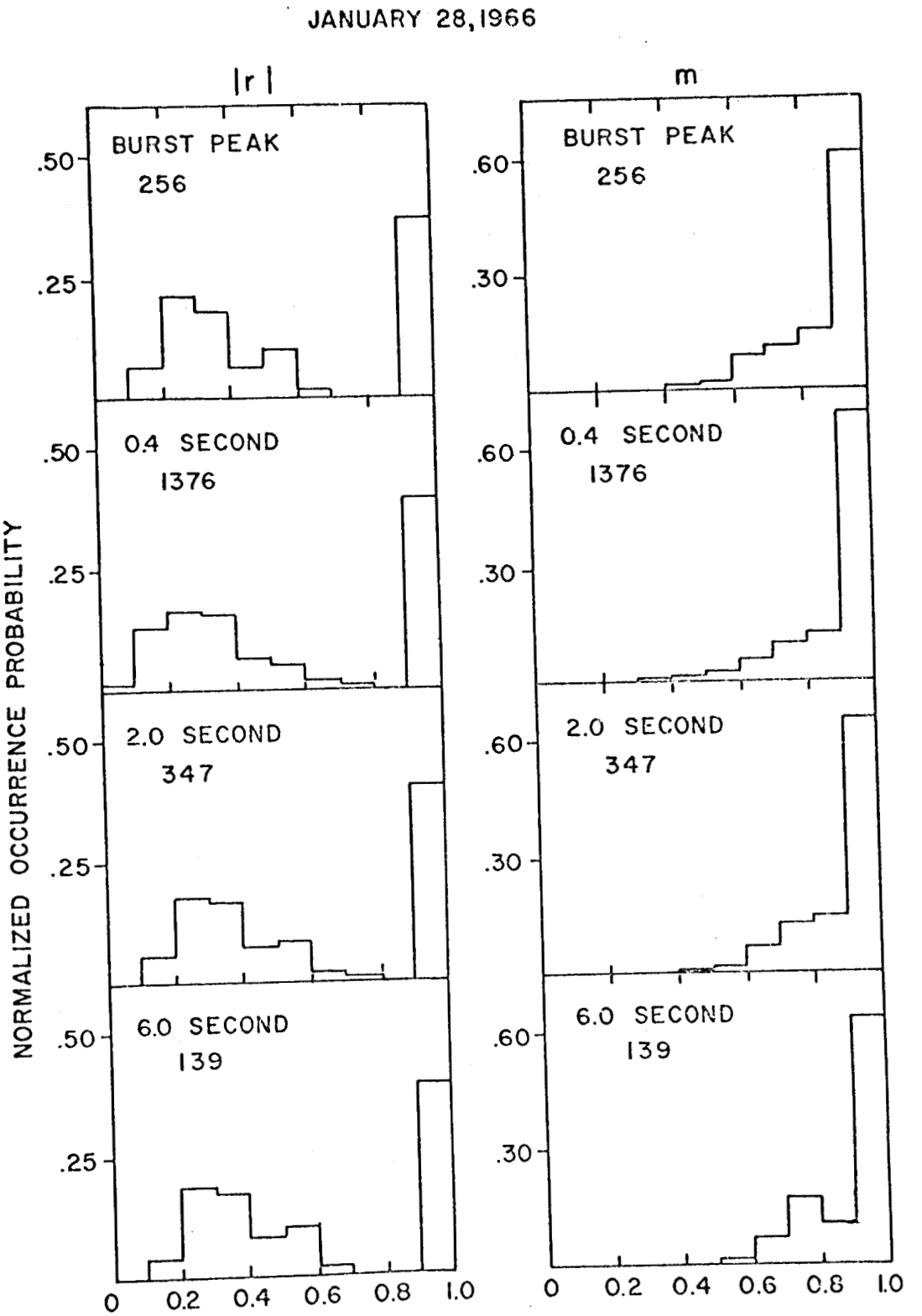

Fig. 16--Distributions of m and |r| for the January 28th event.

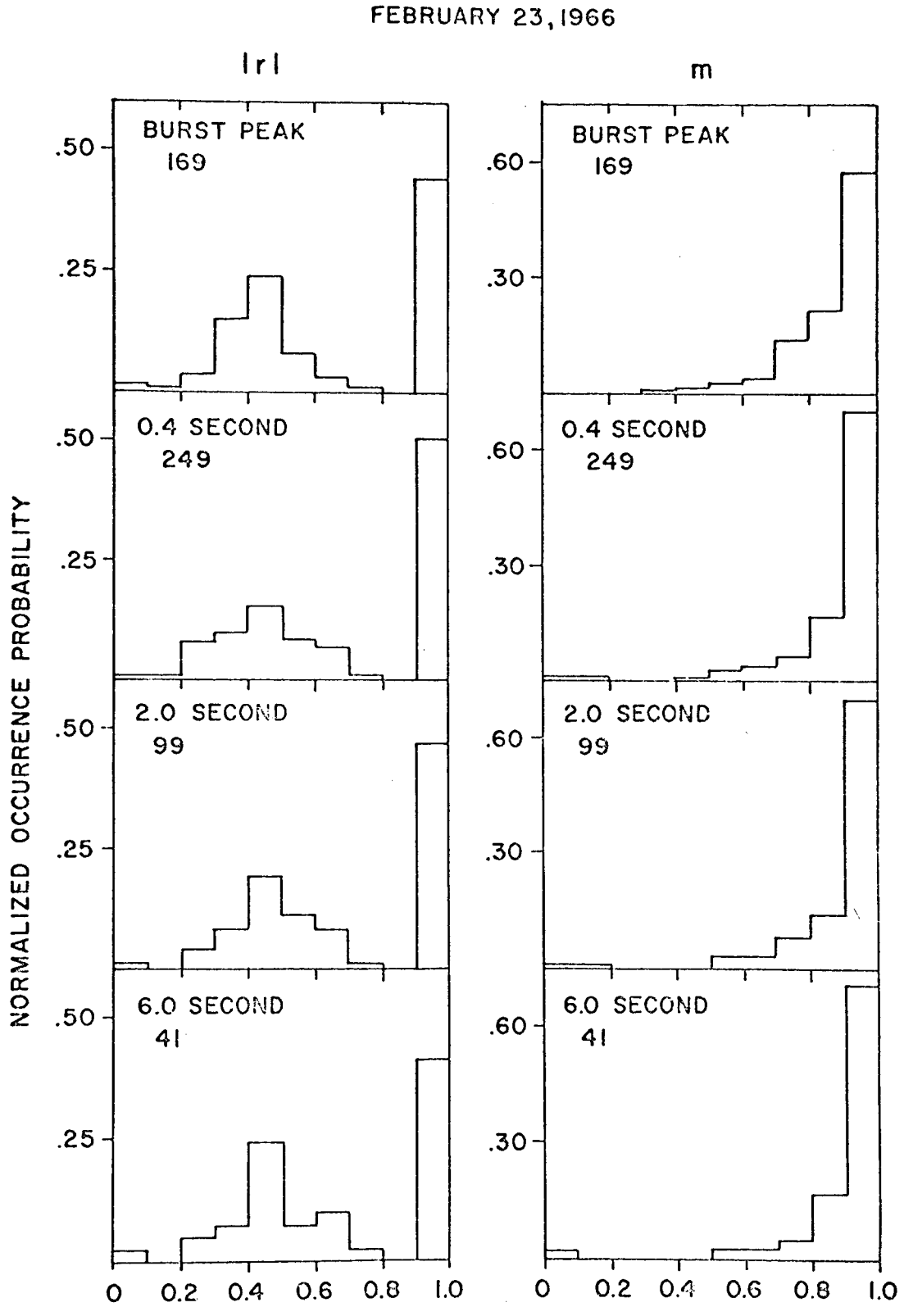

Fig. 17--Distributions of m and |r| for the February 23rd event.

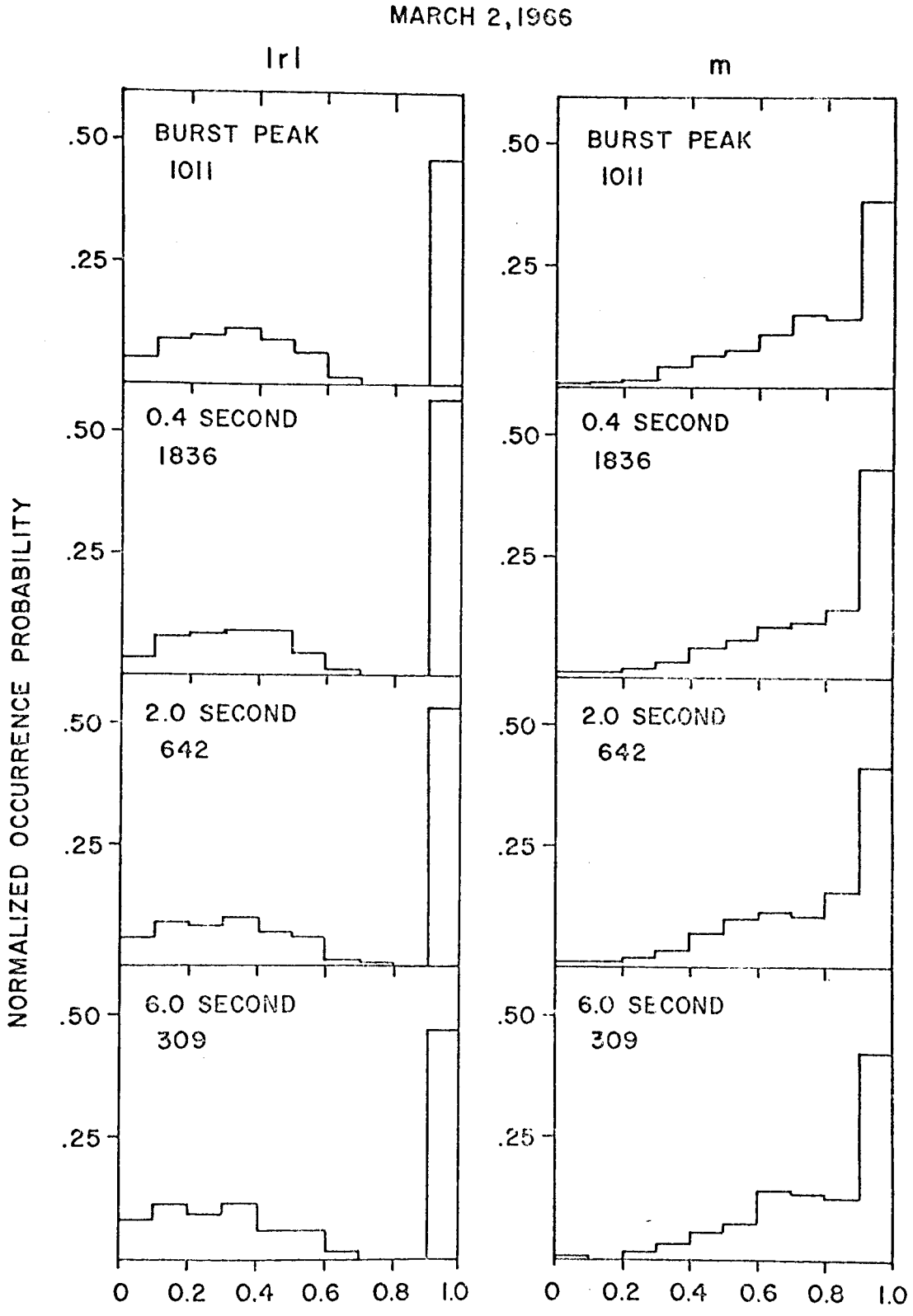

Fig. 18--Distributions of m and |r| for the March 2nd event.

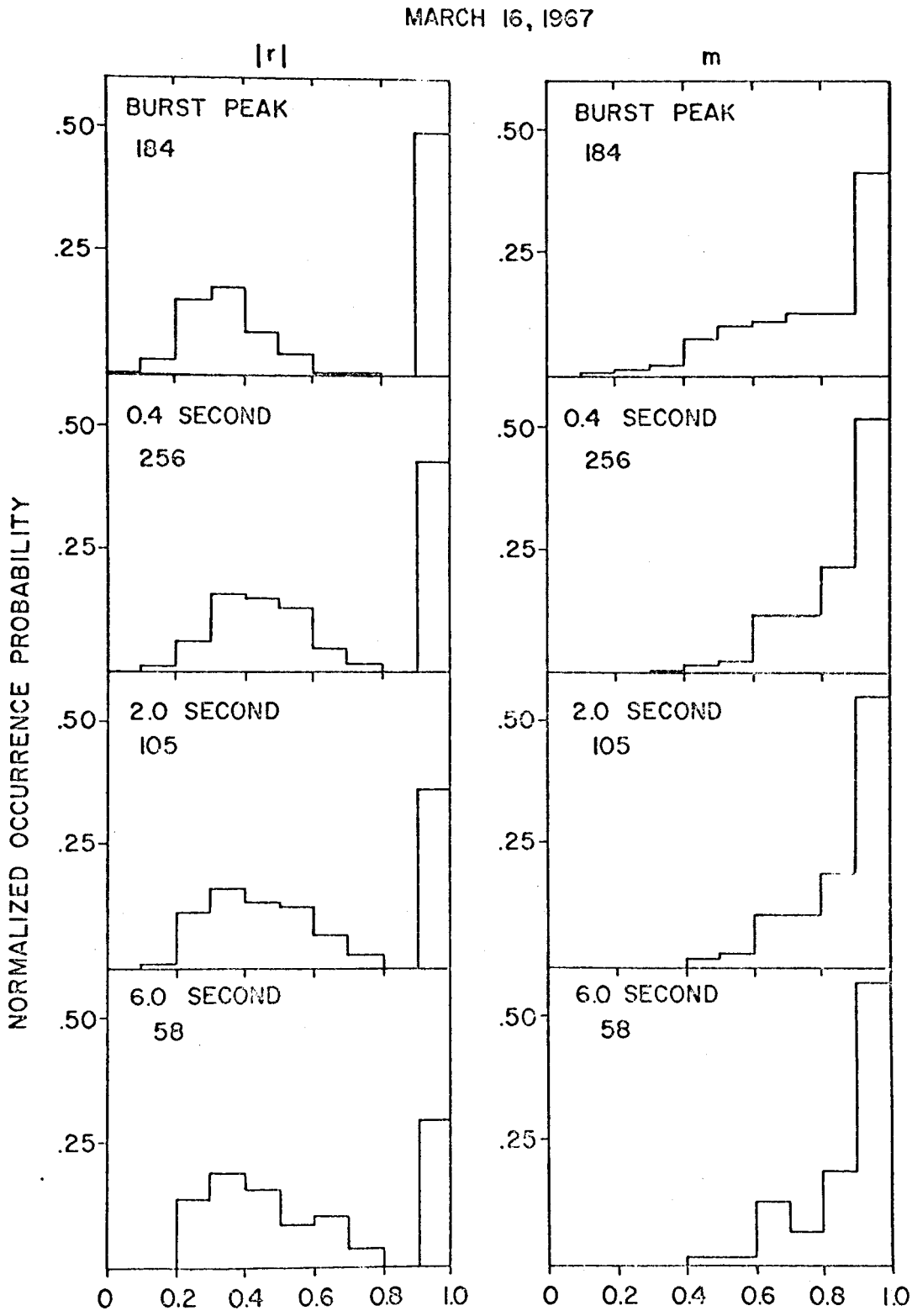

Fig. 19--Distributions of m and |r| for the March 16th event.

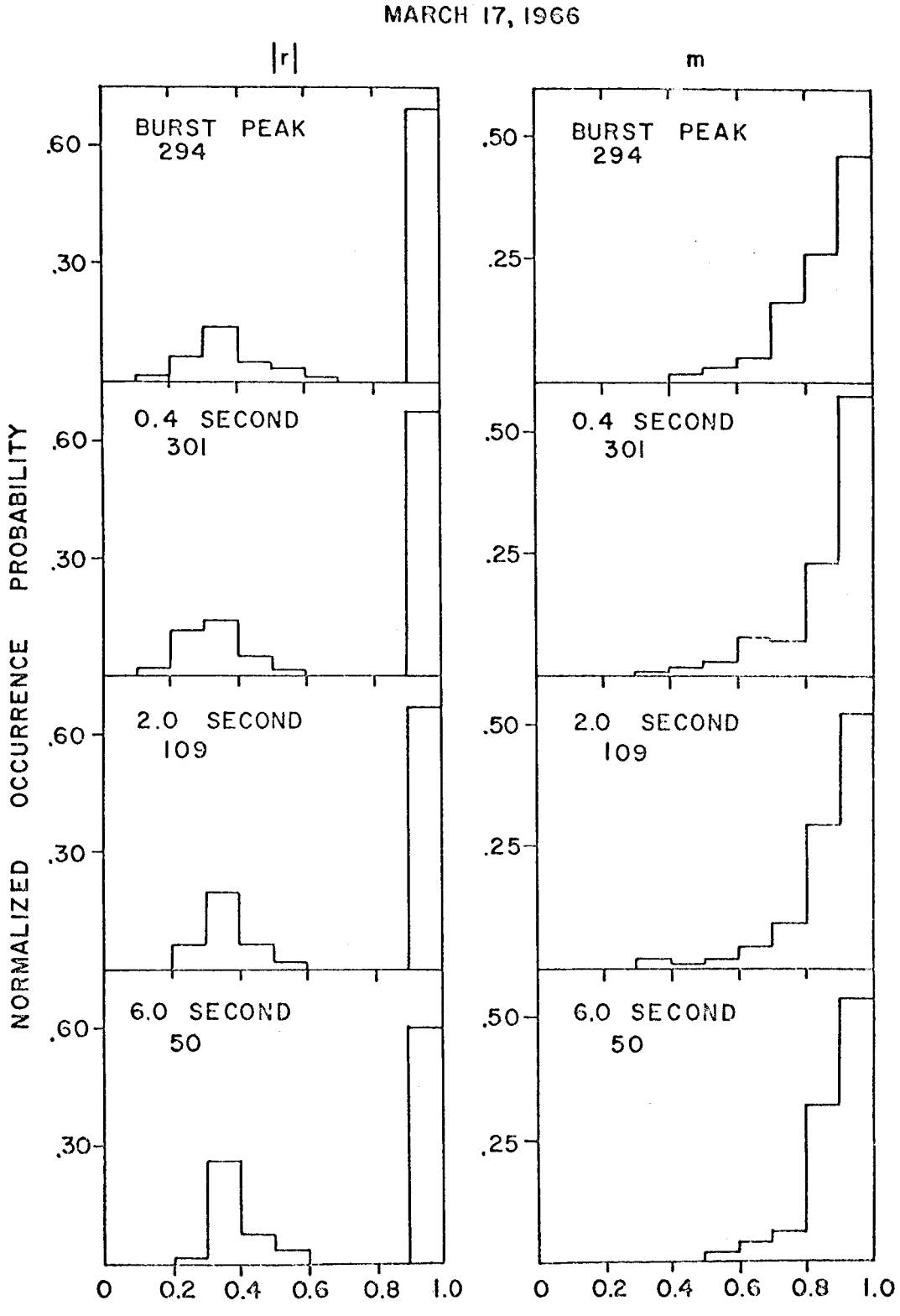

Fig. 20--Distributions of m and |r| for the March 17th event.

each interval by the total number of points contained in the distribution. Table 5 lists the number of points for each analysis for each event.

The drawings indicate that for each event the distributions are roughly the same although the 6.0 second analysis tends to obscure the main features of the distributions. The distributions for the 2.0 second interval analysis seem to contain most of the features of both the burst peak and 0.4 second interval analyses. For every event except the January 28th event the 2.0 second analyses contain fewer points than do the burst analyses. Thus it seems reasonable that future events may be analyzed by a method similar to the 2.0 second analysis and still retain much of the detail and the statistics available with the burst peak studies.

One interesting feature of the diagrams is that about 50% of the bursts consisted of a pure circular component plus a random component ($|r| = 1$ and $m < 1$). Other investigators have also observed that a large proportion of bursts seem to have $|r| = 1$. Since widely differing systems were used it seems clear that this is not an instrumental effect. It is tempting to speculate that perhaps two distinct mechanisms produce the elliptical bursts and the circular bursts. There is, however, no additional support for this position.

VI. ERROR ANALYSIS

It is desirable to put an estimate on the limits of accuracy of the polarization measurements. From Equations 5 we have:

$$m = \frac{I_e}{I_R + I_L}$$

$$r = \tan \beta, \qquad \sin 2\beta = \frac{I_L - I_R}{I_e} \tag{20}$$

$$I_e = \left[(I_L - I_R)^2 + 4 I_{R \cdot L}^2 \right]^{1/2}$$

where I_R, I_L, and $I_{R \cdot L}$ are the currents obtained from the corresponding calibration curves. Using various trigonometric identities, the axial ratio becomes, neglecting the sense of rotation,

$$|r| = \left[\frac{I_e - 2I_{R \cdot L}}{I_e + 2I_{R \cdot L}} \right]^{1/2} . \tag{21}$$

We may consider m and $|r|$ to be functions of the three variables I_r, I_L, and $I_{R \cdot L}$, I_e being a notational convenience.

According to the principle of superposition of errors[38], the error in a quantity Q which is a function of three variables X, Y, and Z is given by:

$$\Delta Q \simeq \frac{\partial Q}{\partial X} (\Delta X) + \frac{\partial Q}{\partial Y} (\Delta Y) + \frac{\partial Q}{\partial Z} (\Delta Z) \tag{22}$$

where ΔX, ΔY, and ΔZ are the errors in X, Y, and Z. If the errors in the variables are independent then the most probable value of ΔQ is given by:

$$\Delta Q = \left[\left(\frac{\partial Q}{\partial X}\right)^2 (\Delta X)^2 + \left(\frac{\partial Q}{\partial Y}\right)^2 (\Delta Y)^2 + \left(\frac{\partial Q}{\partial Z}\right)^2 (\Delta Z)^2\right]^{1/2}. \quad (23)$$

If the measurements of I_R, I_L, and $I_{R \cdot L}$ are independent, then the most probable values of Δm and Δr are given by:

$$\Delta m = \left[\left(\frac{I_R^2 - I_L^2 - I_e^2}{(I_R + I_L)^2 I_e}\right)^2 (\Delta I_R)^2 + \left(\frac{I_R - I_L^2 + I_e^2}{(I_R + I_L)^2 I_e}\right)^2 (\Delta I_L)^2 + \left(\frac{4 I_{R \cdot L}}{(I_R + I_L) I_e}\right)^2 (\Delta I_{R \cdot L})^2\right]^{1/2} \quad (24)$$

$$\Delta r = \left[\left(\frac{4 I_{R \cdot L}^2 (I_R - I_L)^2}{I_e^2 (I_e - 2I_{R \cdot L})(I_e + 2I_{R \cdot L})^3}\right)^2 \left((\Delta I_R)^2 + (\Delta I_L)^2\right) + \frac{4r^2}{I_e^2} (\Delta I_{R \cdot L})^2\right]^{1/2} \quad (25)$$

where the currents I_R, I_L, and $I_{R \cdot L}$ are given by:

$$I_j = \exp(a_j \cdot \mathrm{Ln}(D_j) + b_j), \quad j = R, L, R \cdot L. \quad (26)$$

D_j is the recorder deflection above the background level on the jth

recorder channel and a_j and b_j are the constants obtained from the least-squares construction of the jth calibration curve.

In order to determine whether the errors in the currents are independent and hence whether Equations 24 and 25 are applicable it is necessary to investigate the sources of error. Uncertainties are introduced into the calculations of the durrents by two separate processes involved in the conversion of recorder deflections to currents. The first process is the construction of the calibration curves. The curves were constructed by the method of least squares which has the advantage of providing a statistical estimate of the uncertainty of calculations made from the curve due to the scattering of points about the curve.

The electronics of the antenna-receiver-recorder system guarantees the independence of the I_R and I_L channels; therefore the statistical errors in constructing the calibration curves for these two channels are also independent. Furthermore, since the $I_{R \cdot L}$ channel measures only the product of the amplitudes of the coherent parts of the I_R and I_L signals and since the calibration curve is constructed independently of the curves for the other two channels, the statistical error is independent of the other two channels.

The second process is the determination of D_j in Equation 26 from the record. Since D_j is the deflection above the background level, the background level must be estimated and the recorder deflection must be read from the base line of the chart.

Recorder deflections were read to the nearest half millimeter; thus the deflections are at worst accurate to $\pm$ .5 mm. Estimating the background level was more difficult since fluctuations in the apparent background level were sometimes as much as six millimeters wide on the I_R and I_L channels. If these fluctuations are caused by instrumental noise rather than by weak Jupiter radiation, the background level can be estiamted by measuring the average maximum deflection and the average minimum deflection during a portion of the record when no identifiable Jupiter emission was present. Taking the background level equal to the average of these numbers located the background level to within $\pm$ .5 mm. This procedure was followed for the five events analyzed in Chapter V.

It was found during calibration tests that a change in the simulated background level of as much as one millimeter produced no apparent change in the deflection above the background due to a given current. Therefore the background level, if noise fluctuations are not due to weak Jupiter radiation, is for practical purposes located precisely and the D_j in Equation 26 was taken to be accurate to $\pm$ .5 mm.

Since deflections on different channels were measured sepa - rately, the error due to measuring the deflections on one channel is independent of the error due to measuring the deflection on another channel. Thus all the errors are independent and Equations 24 and 25 are applicable.

In Equations 24 and 25 the quantities ΔI_j occur. These quantities are best estimated by calculating the quantities:

$$I_{j\pm} = \exp(a_j \cdot \mathrm{Ln}(D_j \pm 0.5) + b_j \pm c_j), \quad j = R,\ L,\ R \cdot L \qquad (27)$$

where c_j is the statistical inaccuracy due to the scatter of the calibration points for the jth curve. Then

$$\Delta I_j = \mathrm{Max}(|I_{j\pm} - I_j|). \qquad (28)$$

The quantities $I_{j\pm}$ represent the extreme values which I_j may take on. Hence ΔI_j is the maximum error in the variable I_j.

When ΔI_j is actually computed the fact that the logarithm function is not finite at zero must be considered. This becomes important when $D_j \leq 0.5$ mm. If this happened I_j was arbitrarily set equal to zero. When $I_{R \cdot L}$ was zero, this had a particularly pronounced effect on r. If Equations 21 and 22 are examined, it is seen that when $I_{R \cdot L} = 0$, $r = 1$ from Equation 20 and thus

$$\Delta r = \frac{2\Delta I_{R \cdot L}}{I_L - I_R} . \qquad (29)$$

Now $\Delta I_{R \cdot L}$ is not equal to zero in general and in some cases it may be quite large, particularly on March 2nd, 16th, and 17th where calibration of the records showed that a noise current of about 50 milliamps was required to give a deflection of about 0.5 mm above the background level on the correlator channel. Thus from Equations 24 and 25, $\Delta I_{R \cdot L} \simeq 50$ ma. These points represent pure circular plus random polarization of the radiation since $r = 1$ and comprise about 50%

of the points of the analysis. Using the events of March 2nd, 16th, and 17th as examples $I_L - I_R < 200$ ma for most of these points and hence $\Delta r > 1/2$.

As a result the average Δr for the whole event can be quite high. It can be reduced somewhat by increasing the minimum deflection a point must have to be included in an analysis of a particular event. This was done for various minimum deflections using the initial burst analysis as a basis. Table 6 shows the results of this study for each event.

It is seen from Table 6 that the average value of Δr decreases steadily as a higher minimum deflection is required. Also the average value of Δm decreases in this way except for the event of March 2nd. Calculations of m values for this event revealed that for strongly correlated bursts the m values were greater than 1. Examination of the calibration points for the I_R channel indicated that above about 60 ma an increase in the noise current produced only a small increase in deflection whereas a similar increase in noise current produced a comparatively larger increase in deflection on the I_L channel. This results in a flatter slope for the I_R channel calibration curve and comparatively smaller currents for high deflections than on the I_L channel. This might be accounted for if the diode noise source used to simulate the background level on the I_R channel began to fail at this time. Unfortunately this could not be checked because by the time this

TABLE 6

AVERAGE Δm AND Δr USING BURST ANALYSES FOR VARIOUS MINIMUM DEFLECTIONS (in mm.) WITH $\Delta I_{R \cdot L} \neq 0$

Event	$\overline{\Delta m}$					$\overline{\Delta r}$				
	5.0	7.5	10.0	15.0	20.0	5.0	7.5	10.0	15.0	20.0
January 28	.081	.087	.082	.061	.055	.395	.391	.255	.127	.082
February 23	.115	.093	.079	.063	.057	.216	.118	.091	.061	.053
March 2	.235	.247	.262	.301	.347	.444	.279	.207	.129	.098
March 16	.166	.149	.137	.109	.094	.605	.245	.141	.077	.058
March 17	.113	.096	.083	.067	.059	.619	.477	.363	.177	.144
All Events	.178	.173	.175	.186	.204	.460	.315	.227	.128	.094

event had been analyzed the calibration system then in use had been abandoned for a better one. There is no evidence, however, that this was the case.

Since there were practically no noise fluctuations on the correlator channel, it seems reasonable to say that $\Delta I_{R \cdot L} = 0$ whenever $I_{R \cdot L} = 0$. For this case $\Delta r = 0$. Table 7 shows $\overline{\Delta m}$ and $\overline{\Delta r}$ calculated for each analysis for each event based on this assumption.

During each of the five events analyzed there were small-amplitude signal fluctuations on the I_R and I_L channels throughout the event. They were also found on the correlator channel during the January 28th and February 23rd events and were originally attributed to system noise. However, if these fluctuations were due partially to Jupiter radiation then large systematic errors would be introduced into calculations of m and r and would not be reflected in calculations of error according to Equations 24 and 25.

Since the fluctuations were considered to be system noise, the background level was taken to be the mean of the fluctuations. If the fluctuations were partially of Jovian origin, however, then the background level used for calculations is too high, and hence the currents are too low. If the fluctuations of Jovian origin were linearly polarized, then the polarization fractions are too small and the axial ratios are too high. It is unlikely that the fluctuations represent linearly polarized Jupiter radiation, however, since linearly polarized Jupiter radiation

TABLE 7

AVERAGE Δm AND Δr FOR EACH EVENT AND EACH ANALYSIS

WITH $\Delta I_{R \cdot L} = 0$ WHENEVER $I_{R \cdot L} = 0$

Event	$\overline{\Delta m}$				$\overline{\Delta r}$			
	Burst	0.4 Sec.	2.0 Sec.	6.0 Sec.	Burst	0.4 Sec.	2.0 Sec.	6.0 Sec.
January 28	.087	.149	.109	.092	.021	.021	.022	.022
February 23	.115	.126	.107	.084	.037	.033	.034	.034
March 2	.235	.228	.220	.229	.074	.058	.060	.063
March 16	.166	.151	.146	.141	.040	.018	.023	.029
March 17	.113	.145	.120	.104	.014	.015	.014	.016
All Events	.179	.184	.167	.168	.051	.038	.041	.044

has been observed only rarely and since for three events there were no fluctuations on the correlator channel.

It is more likely that the fluctuations, if truly Jovian in origin, represent random, circular, or elliptical polarizations. In the case of random polarizations the calculated polarization fractions would be systematically high. In the case of circular polarizations the calculated polarization fractions would be systematically low. In neither of the two cases would the axial ratio be affected.

The size of the fluctuations varied considerably from event to event (see Figs. 13-15). The largest occurred during the January 28th event and were about six millimeters wide. For the February 23rd event the width of the fluctuations was about three millimeters and for the remaining events was about 1-1.5 millimeters.

The obvious procedure to resolve this problem would be to extend the record of the event to a point when Jupiter is well out of the reception pattern of the antenna and compare the noise levels of this portion of the record to the noise level during the activity period. Unfortunately, it was not realized that this could be a problem until some time after the events. The records of the events indicate, however, that the fluctuations are instrumental since quite long periods of time during the event contain no identifiable Jupiter activity. The fluctuations during these periods are just as large as the fluctuations during periods when activity is present.

VII. DISCUSSION AND CONCLUSIONS

Figs. 16-20 and Tables 5 and 7 together indicate that within the limits of accuracy of the experiment the 2.0 second interval analysis is as good as the burst peak analysis for events in which the only circularly or elliptically polarized points are either all right-handed or all left-handed. Analysis of the March 2nd event indicates that this is also true of events containing both kinds of polarization. About three per cent of the points in the analyses of the March 2nd event are left circularly or left elliptically polarized; the remainder are right-handed polarized.

The axial ratio and polarization fraction distributions are essentially the same as observed by Dowden, Sherrill, and Barrow. Each of these observers reported a peak in the axial ratio distributions corresponding to pure left or right circularly polarized bursts ($|r| = 1$) containing a substantial number of the points used to construct the distributions. It is tempting to speculate that elliptically polarized bursts have a different origin than circularly polarized bursts but there is no justification for such speculation.

If the circularly polarized bursts are removed from the distributions, the distributions have a shape similar to that predicted by

the Ellis and McCullough theory although they do not fall off as sharply as predicted for values of $|r|$ smaller than the peak value. Dowden observed the same effect and commented that it could be explained by superposition of bursts of opposite sense of polarization. However, the discussion of the time characteristics in Chapter V indicates that superposition is not as serious a problem with the present records.

The effect might be accounted for by crosstalk between the circular component channels. The crosstalk would produce a deflection on the correlator channel because coherent signals would be detected by the product mixer in the receiver. However, if crosstalk is present nearly every burst would appear to be elliptical rather than circular. Furthermore, noise generator tests revealed that there is little or no crosstalk with this polarimeter since simulation of randomly polarized signals with independent noise sources did not change the correlator channel deflection detectably.

According to Ellis and McCullough the location of the peak of the axial ratio distributions for elliptical polarizations is determined by the magnetic latitude of the source region. If the source region were spread over a range of magnetic latitudes the effect would be to broaden and to smooth the peak.

The combined distributions of the five events shown in Fig. 21 represent 1914 bursts detected in an observing time of about 20 hours. As a comparison Sherrill reported 1677 bursts in an observing time of

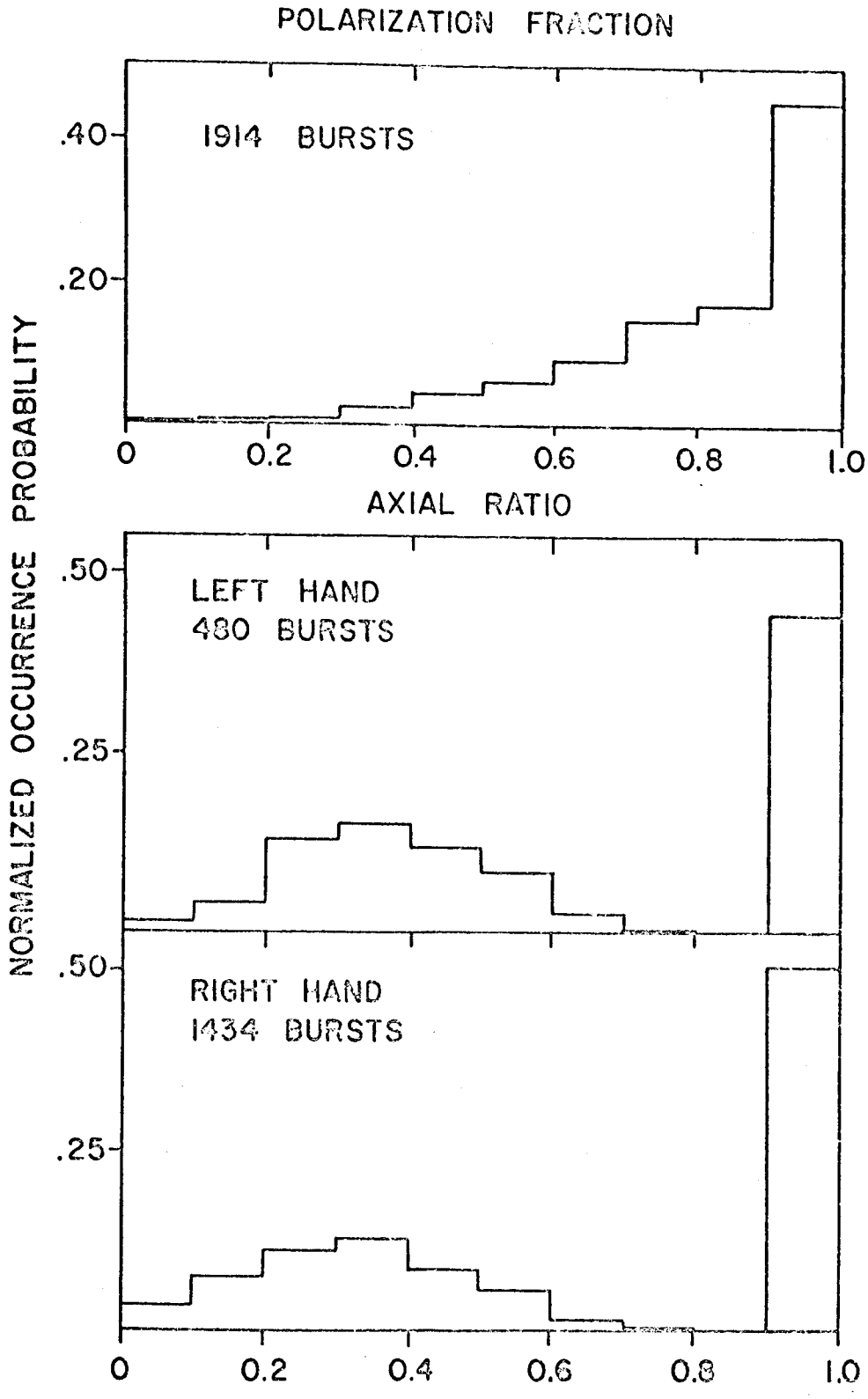

Fig. 21--Distributions of m and |r| for the five events analyzed in Chapter V combined.

48.6 hours. Only about 250 of these were used to construct his polarization fraction and axial ratio distributions. According to Table 5 the distributions for three of the five events analyzed here are as good as or better statistically than Sherrill's distributions for a complete observing season and the remaining two are nearly as good.

Fig. 21 indicates that about 80% of the bursts had a polarization fraction of 0.70 or more. Sherrill found that about 95% of his 18 Mc/s bursts had a polarization fraction of .80 or more. This may perhaps be regarded as some justification for the assumption that $m = 1.0$ made by those observers who recorded only two parameters of polarization.

Various attempts have been made to test the dependence of summed axial ratio on total burst number predicted by the Ellis and McCullough theory. Dowden, Sherrill, and Barrow have tested this prediction by summing the axial ratios of bursts in a given Jovian longitude interval. The summed axial ratio per central meridian longitude region was plotted against the total number of bursts occurring in that region. These observers obtained results consistent with the Ellis and McCullough theory within the limits of accuracy of the observations. In order to obtain sufficient burst numbers it was necessary for these observers to use large longitude intervals and the observations for a complete observing season. For this reason only a limited number of

data points per observing season were available to construct the curve of observed dependence.

The time characteristics of the Florida State University polarimeter make it possible for each event to become a data point because of the larger number of distinguishable bursts per event. Consequently, in a normal observing period a significantly larger number of data points is available. If the method of least squares is used to determine the slope of the observed dependence of summed axial ratio on burst number, the possibility exists of a considerable increase in accuracy of the observed dependence because the statistical uncertainty decreases as the number of data points increases.

The five events listed in Table 4 have each been used as a data point in a log-log plot of $\sum |r|$ versus total burst number N. This is shown in Fig. 22. The slope of the curve is 0.98 ± 0.10 and was obtained by the method of least squares.

No vertical error bars are shown in Fig. 22. If error bars are calculated according to Table 6 for a minimum deflection of five millimeters for the burst analyses, they are found to be very large. For example, for the event of January 28th $\sum|r| = 149.3 \pm 101.2$ and for the event of March 17th, $\sum|r| = 235.3 \pm 182.0$. These events are represented by the two points in Fig. 22 which do not fall close to the calculated curve. If error bars are calculated according to Table 7, they are found to be so small that for the points for the January 28th and

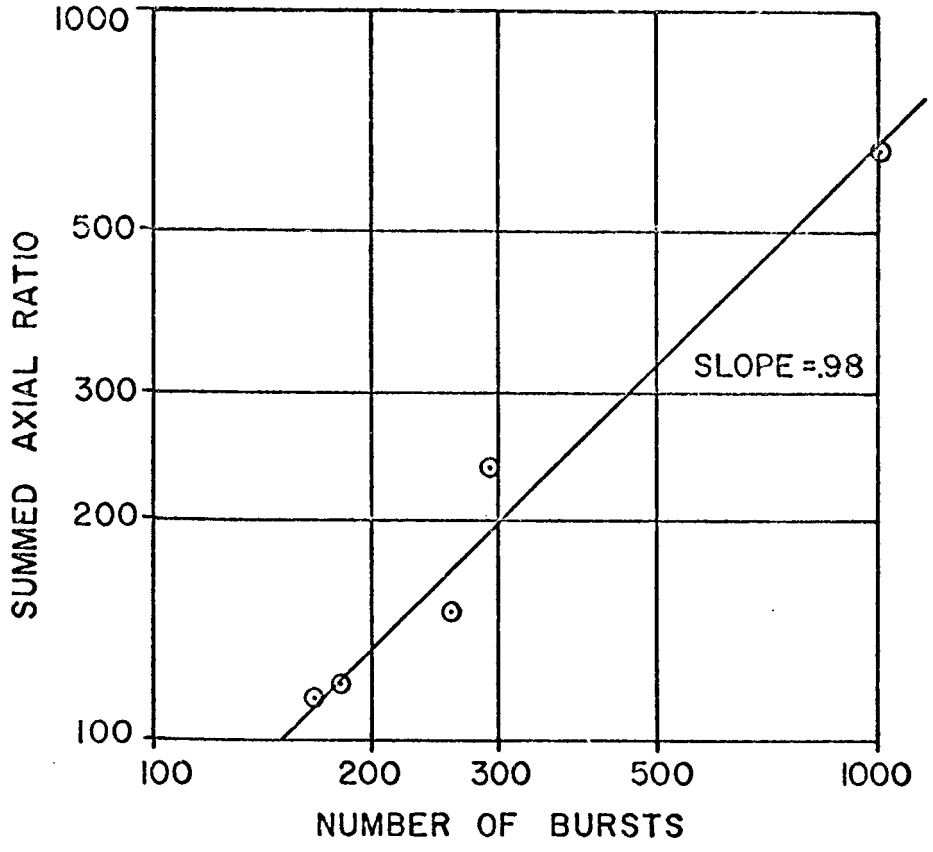

Fig. 22--Summed axial ratio versus number of bursts for the five events analyzed in Chapter V.

March 17th events the error bars would not fall on the curve as drawn, even if the error in calculating the slope of the curve is considered.

The smallest average error $\overline{\Delta r}$ which would permit these points to fall on the curve is about 10% for each. According to Table 6 the largest possible minimum deflection which would give this amount of error is between 15.0 and 20.0 mm for the January 28th event and more than 20.0 mm for the March 17th event. If this criterion is applied to each event, the minimum deflections which could be adopted for each event without allowing the average error to become too large are 15.0 mm for the January 28th event, 7.5 mm for the February 23rd event, 15.0 mm for the March 2nd event, 10.0 mm for the March 16th event, and 20.0 mm for the March 17th event.

The analysis of Chapter VI which led to the production of Table 6 indicated that the very large errors in axial ratio calculations were due to the fact that large currents sometimes produced only a small deflection on the correlator channel. This is because there is a threshold current below which the polarimeter receiver does not work properly. Thus a current of about 8.0 ma was necessary to cause a deflection of 0.5 mm on the correlator channel on February 23rd, about 25.0 ma on January 28th, and about 50.0 ma on March 2nd, 16th, and 17th.

On this basis it is possible to make a preliminary estimate of the minimum deflection which should be chosen for each event. Thus if

a small current produces a detectable deflection on the correlator channel, the analysis should begin with a small minimum deflection such as five millimeters. If it requires a larger current to produce a detectable deflection on the correlator channel, the analysis should begin with a larger minimum deflection.

The foregoing discussion suggests that future observations with the Florida State University polarimeter be made with these points in mind:

1. Analysis of each event which does not contain I-pulses by means of the 2.0 second interval method of analysis.

2. Inclusion in an analysis of an event of only those points with a sufficiently high deflection on at least one circular component channel. (With the Florida State polarimeter system one circular component channel should have a deflection greater than the larger of five millimeters or three times the rms system noise.)

3. Testing the dependence of summed axial ratio on burst number predicted by the Ellis and McCullough theory with a large number of events.

4. Development of a method for testing the dependence of integrated power on number of bursts predicted by the Ellis and McCullough theory.

5. Development of a simpler calibration system. Such a system was established for use during the 1966-1967 apparition of Jupiter. With it the crystal diode noise sources are dispensed with and the signal from the tube noise generator is superimposed over the galactic background at the end of each event. This simplifies the calibration greatly.

REFERENCES

1. C. H. Mayer, T. P. McCullough, and R. M. Sloanaker, Astrophys. J. 127, 1 (1958).

2. C. H. Mayer, T. P. McCullough, and R. M. Sloanaker, Astrophys. J. 127, 11 (1958).

3. R. M. Sloanaker, Astr. J. 64, 346 (1959).

4. B. F. Burke and K. L. Franklin, J. Geophys. Res. 60, 213 (1955).

5. C. A. Shain, Aust. J. Phys. 9, 61 (1956).

6. J. N. Douglas, A Study of Non-Thermal Radio Emission from Jupiter, Ph.D. dissertation, Yale University, 1960.

7. T. D. Carr, A. G. Smith, H. Bollhagen, N. F. Six, Jr., and N. E. Chatterton, Astrophys. J. 130, 105 (1961).

8. International Astronomical Union Information Bulletin 8, March, 1962.

9. E. E. Baart, C. H. Barrow, and R. T. Lee, Nature 211, 808 (1966).

10. T. D. Carr, G. W. Brown, A. G. Smith, C. S. Higgins, H. Bollhagen, J. May, and J. Levy, Astrophys. J. 140, 778 (1964).

11. G. R. A. Ellis, Nature 194, 667 (1962).

12. J. W. Warwick, Astrophys. J. 137, 41 (1963).

13. NASA Jupiter observers Conference, Goddard Space Flight Center, Greenbelt, Maryland, April, 1965.

14. J. N. Douglas and H. J. Smith, Nature 199, 1080 (1963).

15. S. Chandrasekhar, Radiative Transfer (Oxford University Press, London, 1955) pp. 24-35.

16. M. H. Cohen, Proc. I. R. E. 46, 172 (1958).

17. W. M. Sherrill, Astrophys. J. 142, 1171 (1965).

18. K. L. Franklin and B. F. Burke, J. Geophys. Res. 63, 807 (1963).

19. A. G. Smith and T. D. Carr, Astrophys. J. 130, 641 (1959).

20. F. F. Gardner and C. A. Shain, Aust. J. Phys. 11, 55 (1958).

21. C. H. Barrow, Astrophys. J. 135, 847 (1962).

22. T. D. Carr, paper delivered at NASA Jupiter Conference, New York, October, 1962.

23. C. H. Barrow, Nature 201, 171 (1964).

24. W. M. Sherrill and M. P. Castles, Astrophys. J. 138, 587 (1963).

25. R. L. Dowden, Aust. J. Phys. 16, 398 (1963).

26. J. A. Roberts, Planetary and Space Sci. 11, 221 (1963).

27. W. M. Sherrill, Final report Project 06-1358R, Southwest Research Institute, August, 1964.

28. M. H. Cohen, Proc. I. R. E. 46, 183 (1958).

29. J. W. Warwick, Annals New York Acad. Sci. 95, 39 (1961).

30. G. R. A. Ellis, Radio Science J. Res. 69D, 1513 (1965).

31. D. Morris and G. L. Berge, Astrophys. J. 136, 276 (1962).

32. G. L. Berge, Astrophys. J. 146, 767 (1966).

33. G. R. A. Ellis and P. M. McCullough, Aust. J. Phys. 16, 380 (1963).

34. C. H. Barrow, Status Report No. 4 on NASA grant NSG-224-61, January, 1964.

35. C. H. Westcott, Wireless Engineer, July, 1948.

36. J. L. Pawsey and R. N. Bracewell, Radio Astronomy (Oxford University Press, London, 1955), p. 46.

37. R. T. Lee, M. S. thesis, Florida State University, 1966.

38. J. Topping, Errors of Observation and Their Treatment (Reinhold Publishing Corporation, New York, 1960), pp. 19-20.